NONLINEAR SOFTENED STRUT-AND-TIE MODEL FOR SEISMIC SHEAR RESISTANCE OF R.C. BEAM-COLUMN JOINTS

F.B.A. Beshara, I.M. Bazan, Y.H. Hammad, and A.S. Abd El-Maula

Faculty of Engineering, Shobra, Zagazig University

Abstract

For predicting the shear strength and failure mechanism of the beam-column joint cores in reinforced concrete ductile frames under seismic loads, a nonlinear softened strut-and-tie model has been developed in this paper. The proposed unified model for exterior and interior joints is derived to satisfy equilibrium, strain compatibility, and the constitutive laws of cracked concrete and steel. The intended approach addresses all critical shear components within the joint, and a statically indeterminate load pattern has been chosen before and after yielding of the steel reinforcement within the joints. The macro-model of the diagonal compression strut of concrete depends on the effective joint dimensions and the level and type of column load. The horizontal and vertical ties are made-up of the joint hoops, the column intermediate bars, and the inclined joint bars. Depending on the distribution pattern and bond condition, the model accounts for the unequal participation of joint reinforcement in shear resistance. The nonlinear compression law for concrete considers the effects of the hoops-induced confinement and the cracking-related softening. For reinforced concrete in tension, the composite law accounts for the influence of concrete cracking, tension stiffening, and yielding of steel ties. The accuracy of the proposed procedure was checked by comparing the calculated shear strengths with the experimental data reported in literature, and a satisfactory correlation was found. Extensive parametric studies were performed to provide valuable insights into the strength behavior and design of the exterior and interior joints under seismic loading.

ملخص البحث

يختص هذا البحث بتطوير نموذج تحليلى لاخطى باستخدام نموذج (دعامة/شداد) الملين لحساب المقاومة القصية وآليات الانهيار لقلب وصلات الكمرات والأعمدة الخرسانية المسلحة تحت تأثير أحمال الزلازل. وقد تم اشتقاق النموذج المقترح الموحد للوصلات الداخلية والخارجية بحيث أن يحقق شروط اتزان القوى وتوافق الانفعالات والقوانين البنائية للخرسانة المشرخة والحديد. يتناول الأسلوب المقدم كل مركبات المقاومة القصية بالوصلة مع استخدام نمط تحميلى غير محدد استاتيكياً قبل وبعد خضوع حديد التسليح بالوصلة. ويعتمد تمثيل الدعامة الخرسانية القطرية على أبعاد الوصلة الفعالة ومستوى ونوع حمل العمود، وتتكون الشدادات الأفقية والرأسية من كانات الوصلة والحديد الأوسط للعمود وأيضاً الأسياخ المائلة بالوصلة إن وجدت مع الأخذ فى الاعتبار تأثير الاشتراك غير المتساوى فى المقاومة القصية وذلك اعتماداً على نمط التوزيع وشروط التماسك لحديد التسليح. يأخذ قانون الخرسانة البنائى للضغط تأثير آلية التحزيم للكانات وكذلك آلية التلين

المصاحبة لتشرخ الخرسانة. كما يتناول القانون البنائى المركب فى الشد تأثير التشريخ وتصلب الشد وخضوع حديد التسليح. بمقارنة النتائج التحليلية بأخرى تجريبية من مصادر مرجعية، وجد أن هناك توافق جيد بين النتائج مما يشير إلى دقة النموذج المقترح. وأخيراً تم إجراء دراسات بارامترية شاملة للعوامل المختلفة التى تؤثر على مقاومة وسلوك وتصميم الوصلات الداخلية والخارجية تحت تأثير الزلازل.

1. Introduction

During the past three decades, a great deal of experimental research on beam-column joints in reinforced concrete moment-resisting frames under seismic excitations, has been conducted [1-30] in several countries. Based on these tests, design recommendations have been developed and incorporated into current codes [31-37]. Under earthquake loads, the joint region is subjected to horizontal and vertical shear forces whose magnitudes are typically higher than those within the adjacent beams and columns. If the joint design is not carefully performed, the beam-column joint may become the weakest link in lateral resistance of frames. A code-specified level of shear strength can be achieved only if the joint is detailed according to the code. Therefore, it is difficult for designers to determine when particular joint detail may adversely affect the shear strength. Also, the empirical procedure of design codes leads to different amounts and arrangement of transverse reinforcement in joints and construction problems are often practically experienced. Another major concern [35-37] is that the recommended design approaches may vary significantly in the determination of joint shear strength. The New Zealand Code [33] postulates two kinds of resisting joint mechanisms as the diagonal strut and the truss mechanisms. U.S. and Japanese standards [31,32] state implicitly that it is only necessary to consider the diagonal strut mechanism. In the literature [35-39], some simple analytical models have been used to provide an alternative approach for the shear behavior of joints.

The objective of the present paper is to develop a nonlinear softened strut-and-tie model for predicting the seismic shear resistance and failure mechanism of the beam-column joints. Using a rational and unified approach, the proposed model satisfies equilibrium, strain compatibility, and the nonlinear constitutive laws of concrete and steel. The macro-modeling of concrete strut and steel ties depends on the joint geometry, reinforcement and loading conditions. The constitutive laws accounts for the concrete nonlinearities in compression and tension, yielding and bond conditions of reinforcement. The proposed analytical model is used to predict the shear strength of several joints tested before, and to perform necessary parametric studies.

2. Derivation of the softened strut-and-tie model

2.1 External actions and internal shear forces at joints

The earthquakes induced forces acting on an interior joint are identified in Figure (1). The horizontal joint shear force (Q_h) may be calculated from the equilibrium of forces in the horizontal direction at the mid-depth of the joint as:

$$Q_h = T_{b1} + C_{b2} - Q_{c1} \tag{1}$$

T_{b1} is the tensile force in the steel of the beam at the right of the joint; C_{b2} is the compression force resulting from the compressive zone of the beam at the left of joint; and Q_{c1} is the horizontal column shear above the joint. For exterior joint where the beam of the left side does not exist, the compression force C_{b2} is zero. Considering the dimensions of the beam and column tension-compression couples, the rectangular area bounded by dashed lines in Figure (1), is regarded as shear element. The intensity of the vertical joint shear force can be approximated by:

$$Q_v = (y_{ctb} / y_{ctc}) \; Q_h \tag{2}$$

where y_{ctb} and y_{ctc} are the internal lever arms in the beams and columns, respectively. The column axial load coupled with moment increase the vertical joint shear force (Q_v) and decrease the internal lever arm in the column.

Under the internal joint forces, the cracks are formed perpendicular to the principal tensile stress direction. As a result, diagonal cracks are formed in the joint core. By considering the core as a cracked reinforced concrete membrane, the states of stress and strain are defined in an average manner, as shown in Figure (2). σ_d is the average compressive stress of concrete in the principal d-direction. σ_r is the average concrete tensile stress in the principal r-direction. ε_d and ε_r are the average principal strains in d- and r-directions respectively. σ_h and σ_v are the average tensile stresses in the horizontal and vertical joint reinforcements respectively. ε_h and ε_v are the average steel strains.

2.2 **Macro-model of beam-column joint**

Statically indeterminate strut-and-tie load paths are proposed to model the force transferring within the joint. The proposed model composes of the diagonal, horizontal and vertical mechanisms. As depicted in Figure (3), the diagonal mechanism is a single diagonal compression strut whose direction is assumed to coincide with the direction of the principal compressive stress of concrete. The angle of inclination of the strut (θ) is defined by:

$$\theta = \tan^{-1} (h_b / h_c) \tag{3}$$

where h_b is the distance between the extreme longitudinal beam reinforcement. For the interior joint (Figure 3-a) as well as for exterior joint with beam stub (Figure 3-c), h_c is the distance between the extreme longitudinal reinforcement in the column. Because the exterior joint without beam stub (figure 3-b), may not fully engaged due to the required hook dimension, h_c is measured as the distance between the centroid of extreme longitudinal column reinforcement to the centroid of beam bar extension at the free end of the 90 degree hooked bar. Generally the formation of the diagonal strut depends on the end condition provided by the compression zone in beams and columns. In the definition of the effective area of the diagonal strut, the following points are considered:

1-   The width of the diagonal strut (b_s) is taken as the effective width of the joint (b_j) which is defined in [31,34].

2-   For ductile beam-column joints where a beam hinge occurs at the face of the column, the spalling of the compression zone in the beam is frequently observed. Since the crushing produces a small compression zone in the beam, the depth of a strut (a_s) can be estimated as equal to the depth of the compression zone in the column ($a_s = a_c$).

3-   Under column compression load, the internal tensile stresses at the horizontal centerline of the joint are reduced and the diagonal compression force will be large. In this situation, the depth of flexural compression zone of the elastic column can be approximated [37] by:

$$a_c = 0.25 \ (1 + 3.4 \ \frac{N}{A_g f_c'}) \ t_c \tag{4}$$

where N is the axial compression load acting on the column, f_c' is the compressive strength of concrete, A_g is the gross area of column section and t_c is the column thickness in the direction of loading.

4-   Recent studies [28] have shown that axial column tension may be experienced by intermediate stories of medium to high-rise building as a consequence of high overturning moments coexisting with vertical ground motion. In this case, concrete contribution to shear can not be fully relied on. In the absence of sufficient data, the depth of the strut under column tension is proposed here by:

$$a_c = 0.25 \ (1 - 4 \ \frac{N}{A_g f_c'}) \ t_c \tag{5}$$

Based on the above considerations, the effective area of the diagonal strut (A_{strut}) is found as:

$$A_{strut} = 0.25 \ (1 + \xi \ \frac{N}{A_g f_c'}) \ b_j \ t_c \tag{6}$$

where ξ is taken as (3.4) for column under compression and (− 4.0) for column under tension.

With reference to Figure (4-a), the horizontal mechanism is composed of one horizontal tie and two flat struts. Also, the proposed vertical mechanism contains one vertical tie and two steep struts, Figure (4-b). The horizontal tie and vertical tie are generally made up of the joint hoops, the intermediate column bars, and joint inclined bars. In the definition of the effective areas of the ties, the following conditions are made:

1-   Unequal participation of the joint hoops and column bars in resisting shear forces was experimentally observed [37]. For estimating the cross area of the horizontal tie, the joint hoops within the center half of the joint core are considered fully effective and other joint hoops are included at a rate of 50%.

2-   Available test results [11] showed that the use of cross inclined reinforcing bars in joint region is one of the most effective ways to improve the seismic resistance of reinforced concrete beam-column joints. As shown in Figure (4-c), the presence of

inclined bars introduces an additional truss action to the shear resisting mechanisms. The determination of the portion of shear carried by inclined bars (F_{inc}) is determined from force analysis.

From the above points, the effective area of the horizontal tie (A_{th}) and vertical tie (A_{tv}) in a joint is calculated as:

$$A_{th} = n_{eh} (A_{hs1} + 0.75 A_{hs2}) + 2 A_{inc} \sin \psi \qquad (7)$$

$$A_{tv} = n_{ev} (A_{vs}) + 2 A_{inc} \cos \psi \qquad (8)$$

in which A_{hs1} is the sectional area of the branches of the main hoop with 90 degree, and A_{hs2} is the area of the branches of cross ties (diagonal-shaped and octagonal-shaped ties). The effective number of layers of joint hoops (n_{eh}) and the effective number of layers of intermediate column bars (n_{ev}), are determined from Figure (5) [39] using the corresponding total number of hoops (n_{th}) and bars (n_{tv}). A_{inc} is the area of inclined bars; and ψ is the inclination of these bars to the column axis.

2.3 <u>Equilibrium conditions of joint forces</u>

Using the proposed strut and tie model for a beam-column joint, Figure (6) demonstrates the forces acting on joint region and forces acting on nodes at maximum response. From force equilibrium at section 1-2 and section 1-3, the resistances against the horizontal joint shear (Q_h) and vertical joint shear (Q_v) can be expressed respectively as:

$$Q_h = D \cos \theta + F_h + F_v \cot \theta \qquad (9)$$

$$Q_v = D \sin \theta + F_h \tan \theta + F_v \qquad (10)$$

in which D is the compression force in the diagonal strut; F_h is the tension force in the horizontal tie; and F_v is the tension force in the vertical tie. There are three load paths in the joint region, and the joint shear forces must be apportioned to the resisting mechanisms. The ratios of the horizontal shear (Q_h) and the vertical shear (Q_v) assigned among the three mechanisms are assumed as:

$$D \cos \theta : F_h : F_v \cot \theta = R_d : R_h : R_v \qquad (11)$$

$$D \sin \theta : F_h \tan \theta : F_v = R_d : R_h : R_v \qquad (12)$$

where R_d, R_h, and R_v are the ratios of the joint shears resisted by the diagonal, horizontal, and vertical mechanisms, respectively. Based on the previous work of Schafer [42], these ratios were derived from the study of statically indeterminate tie forces in reduced mechanisms due to the absence of the horizontal tie or the vertical tie. The values of these ratios are defined as:

$$R_d = (1-\gamma_h) (1-\gamma_v)/(1-\gamma_h \gamma_v) \qquad (13)$$

$$R_h = \gamma_h (1-\gamma_v)/(1-\gamma_h \gamma_v) \qquad (14)$$

$$R_v = \gamma_v \ (1-\gamma_h)/(1-\gamma_h\gamma_v) \qquad\qquad (15)$$

$$R_{tot} = R_h + R_v + R_d \qquad\qquad (16)$$

where γ_h is the fraction of horizontal shear carried by the horizontal tie with the absence of the vertical tie; and γ_v is the fraction of vertical shear carried by the vertical tie with the absence of the horizontal tie. The values of γ_h and γ_v are assigned [42] as:

$$\gamma_h = \frac{2\tan\theta - 1}{3} \qquad\qquad \text{for} \ \ 0 \le \gamma_h \le 1 \qquad\qquad (17)$$

$$\gamma_v = \frac{2\cot\theta - 1}{3} \qquad\qquad \text{for} \ \ 0 \le \gamma_v \le 1 \qquad\qquad (18)$$

Considering that the sum of R_d, R_h, and R_v equals unity ($R_{tot} = 1.0$), equation (11) can be related as:

$$D = (R_d/R_{tot})(Q_h/\cos\theta) \qquad\qquad (19)$$

$$F_h = (R_h/R_{tot}) \ Q_h \qquad\qquad (20)$$

$$F_v = (R_v/R_{tot})(Q_h/\cot\theta) \qquad\qquad (21)$$

The bond strength between longitudinal reinforcement and joint core concrete deteriorates under reversal cyclic loading [37]. However, the complete loss of bond along the beam reinforcement, may impair the development of the vertical mechanism, since the horizontal force needed for equilibrium of vertical tie and steep struts (Figure 6) is missing. To account for the effect of complete bond slip cases in the proposed model, it is suggested to remove the vertical mechanism from the shear resistance by setting ($A_{tv} = 0$) in the analysis. Also, the internal joint forces should be modified under varied yielding conditions of the tie.

2.4 <u>Constitutive law of confined concrete in compression</u>

The constitutive law of concrete is used to evaluate the compressive stresses and strains in the struts. It is assumed that one of the principal axes coincides with the direction of diagonal concrete strut. To enhance the understanding of the shear problem of joints, the following crucial characteristics are involved in the proposed stress-strain curve of concrete:

1- Softening of compression curve as a result of transverse tensile strain and cracking.
2- Improvement of compressive response due to the confinement of concrete by stirrups.
3- The effect of strength level on the shape of compression curve.

The proposed softened stress-strain curve for confined concrete is shown in Figure (7). The properties of the ascending and descending branches of the curve are based on the uncracked confined concrete model of [43]. Some modifications are made here due to consider of the effects of compression softening and concrete grade. The ascending part is represented by the widely used second-degree parabola as follows:

$$\sigma_d = \beta \ k \ f_c' \left[2\left(\frac{\varepsilon_d}{\beta k \varepsilon_o}\right) + \left(\frac{\varepsilon_d}{\beta k \varepsilon_o}\right)^2 \right] \qquad \text{for} \ \left(\frac{\varepsilon_d}{\beta k \varepsilon_o}\right) \leq 1 \qquad (22)$$

$$k = 1 + \frac{\rho_s \, f_{yh}}{f_c'} \qquad\qquad (23)$$

$$\beta = \frac{5.8}{\sqrt{f_c'(1 + 400 \varepsilon_r)}} \quad \leq \quad \frac{0.9}{\sqrt{1 + 400 \varepsilon_r}} \qquad\qquad (24)$$

where f_c' is the compressive strength of unconfined concrete in units of MPa; and β is a semi empirical softening parameter, as proposed in [44]. The factor, k accounts for the strength and ductility increase due to confinement mechanism. f_{yh} is the yield stress of stirrups and ρ_s is the volume of hoop reinforcement to the volume concrete core measured to outside of stirrups. The strain at the peak stress ε_o , is defined [38] for unconfined normal and high strength concrete as:

$$\varepsilon_o = 0.002 + 0.001 \frac{f_c' - 20}{80} \qquad \text{for} \ \ 20 \leq f_c' \leq 100 \ \text{MPa} \qquad (25)$$

The post-peak range is represented by a linear branch as follows:

$$\sigma_d = \beta k \, f_c' \left[1 - Z \, (\varepsilon_d - \beta \, k \, f_c') \right] \qquad\qquad \text{for} \ \ \varepsilon_d \leq \varepsilon_u \qquad (26)$$

$$Z = 0.5 / (\varepsilon_{cc} + \varepsilon_{ch} - \beta k \varepsilon_o) \qquad\qquad (27)$$

$$\varepsilon_{cc} = \frac{3 + 0.29 \, \beta \, f_c'}{145 \, f_c' - 1000} \qquad\qquad (28)$$

$$\varepsilon_{ch} = 0.75 \ \rho_s \ \sqrt{(b_c / s)} \qquad\qquad (29)$$

where Z is the downward slope of the falling branch; b_c is the width of confined core, and s is the spacing of stirrups. The definition of strains of ε_{cc} and ε_{ch} accounts for the effects of concrete strength and confinement respectively on the curve shape. The ultimate strain ε_u is assumed to be 2.5 times the strain at peak stress as a reasonable limit in the calculation of plastic deformations in R.C. connections. The effect of confinement is lost if the transverse steel yields during joint loading.

2.5 Constitutive law of steel and tension stiffening

The behavior of bare steel bars is usually assumed to be elastic-perfectly plastic. However, after cracking, concrete between the cracks still carries tensile stress which is transferred through bond between the reinforcement and the surrounding concrete. To account for the tension stiffening effect on the interactive behavior, the average tensile stress-strain relationship of concrete in the r-direction is shown in Figure (8) and is expressed [44] by:

$$\sigma_r = E_c \, \varepsilon_r \qquad\qquad\qquad \varepsilon_r \leq \varepsilon_{cr} \qquad\qquad (30)$$

$$\sigma_r = f_{tu} \, \left(\varepsilon_{cr}/\varepsilon_r\right)^{0.4} \qquad\qquad \varepsilon_y > \varepsilon_r > \varepsilon_{cr} \qquad\qquad (31)$$

$$\varepsilon_{cr} = f_{tu}/E_c \qquad\qquad\qquad\qquad\qquad (32)$$

in which ε_{cr} is the crack initiation strain in r-direction, and ε_y is the yield strain of steel. For concrete, the elasticity modulus and tensile strength are given as empirical functions of concrete strength [31,34]. The modular ratio is defined as the ratio between the steel elasticity modulus E_s and the secant modulus of elasticity of concrete. Before cracking, this ratio (m) is expressed by:

$$m = E_s/E_c \qquad\qquad\qquad\qquad \varepsilon_r \leq \varepsilon_{cr} \qquad\qquad (33)$$

From equations (31,32,33), the modular ratio after cracking (n) is expressed as:

$$n = m \, \left(\varepsilon_r/\varepsilon_{cr}\right)^{1.4} \qquad\qquad \varepsilon_y > \varepsilon_r > \varepsilon_{cr} \qquad\qquad (34)$$

An alternative approach for simulating the tension stiffening effect in the proposed model is to increase the stiffness and stress of steel ties. This additional steel stress represents the total tensile force carried by both the steel and concrete between the cracks. This added stress is lumped at the level of steel and oriented in the same direction of reinforcement. At steel yielding, the stiffening contribution is practically zero. As shown in Figure (9), the tension stiffening curve (ABC) is added to the elasto-plastic steel curve (ACD) such that:

$$\sigma_s = \phi \, E_s \, \varepsilon_s \qquad\qquad\qquad \varepsilon_s \leq \varepsilon_y \qquad\qquad (35)$$

$$\sigma_s = f_y \qquad\qquad\qquad\qquad \varepsilon_s \geq \varepsilon_y \qquad\qquad (36)$$

where ϕ is the tension stiffening factor; and σ_s and ε_s are the average steel stress and strain. As shown in Figure (9), part AB is before concrete cracking and the curve BC is after cracking. The relationship between forces and strains of the tension ties can be constructed as:

$$F_h = A_{th} \, \phi_h \, E_s \, \varepsilon_h \qquad\qquad F_h \leq F_{yh} \;,\quad F_{yh} = A_{th} \, f_{yh} \qquad (37)$$

$$F_v = A_{tv} \, \phi_v \, E_s \, \varepsilon_v \qquad\qquad F_v \leq F_{yv} \;,\quad F_{yv} = A_{tv} \, f_{yv} \qquad (38)$$

where F_{yh} and F_{yv} are the yielding forces of the horizontal and vertical ties, respectively. f_{yh} and f_{yv} are the corresponding yield stresses of steel ties.

Using the principals of minimum resistance and composite theory, the tension stiffening factors for an orthogonally reinforced element with diagonal cracks were derived in [45] in terms of the concrete modulus. Using equations (33,34), these relations are modified here for the horizontal and vertical ties as:

$$\phi_h = 1 + \left(\frac{1}{m_h \, \rho_h}\right) \qquad\qquad \varepsilon_r \leq \varepsilon_{cr} \;,\quad \varepsilon_h < \varepsilon_{yh} \qquad (39)$$

$$\phi_h = 1 + \left(\frac{\sin^4 \theta}{n_h \, \rho_h} \right) \qquad \varepsilon_r > \varepsilon_{cr} \ , \ \varepsilon_h < \varepsilon_{yh} \qquad (40)$$

$$\phi_v = 1 + \left(\frac{1}{m_v \, \rho_v} \right) \qquad \varepsilon_r \leq \varepsilon_{cr} \ , \ \varepsilon_v < \varepsilon_{yv} \qquad (41)$$

$$\phi_v = 1 + \left(\frac{\cos^4 \theta}{n_v \, \rho_v} \right) \qquad \varepsilon_r > \varepsilon_{cr} \ , \ \varepsilon_v < \varepsilon_{yv} \qquad (42)$$

For the horizontal tie, m_h, n_h and ρ_h are respectively the uncracked modular ratio, the cracked modular ratio and the horizontal reinforcement ratio. m_v, n_v and ρ_v are the corresponding values for the vertical tie.

2.6 Strain compatibility conditions

The relationship among the average strains in different coordinate systems is expressed by the two-dimensional compatibility condition. Accepting the predetermined direction of the principal compression stresses θ, the principal tensile strain (ε_r) can be related to the horizontal strain (ε_h), the vertical strain (ε_v) and the magnitude of the principal compressive strain (ε_d). The transformation of the average strains between h-v coordinate system and d-r principal axes expresses ε_r as:

$$\varepsilon_r = \varepsilon_h + (\varepsilon_h - \varepsilon_d) \ \cot^2 \theta \qquad (43)$$

$$\varepsilon_r = \varepsilon_v + (\varepsilon_v - \varepsilon_d) \ \tan^2 \theta \qquad (44)$$

Also, the equality condition of the Mohr's circle of the average strain states that the sum of the normal strains in the perpendicular direction is a constant.

$$\varepsilon_r + \varepsilon_d = \varepsilon_h + \varepsilon_v \qquad (45)$$

Equations (43,44) are used to estimate the value of principal tensile strain ε_r which is directly related to the softening of concrete. The average shear strain in the joint core is also given by:

$$\gamma_{hv} = 2 \ (\varepsilon_r - \varepsilon_d) \ \sin \theta \ \cos \theta \qquad (46)$$

3. Computational procedure of the nonlinear analytical model

3.1 Yielding and failure conditions

The varied yielding conditions of the steel ties, before the concrete strut is approaching its compressive capacity, results in five solution algorithms described as follows:

1-   **Type YH ($F_h = F_{yh}$ and $F_v < F_{yv}$):** It deals with the case that the yielding of the horizontal tie precedes the reaching of the concrete strength but the vertical tie is still effective in constraining the cracks.

2-   **Type YV ($F_h < F_{yh}$ and $F_v = F_{yv}$):** It treats the case that yielding of vertical tie precedes the reaching of the concrete strength, whereas horizontal tie is still in the elastic range.

3-   **Type YHV ($F_h = F_{yh}$, and then $F_v = F_{yv}$):** It includes the case where the yielding of the horizontal tie occurs first, then the vertical tie yields, and finally the concrete strut arrives at its capacity.

4-   **Type YVH ($F_v = F_{yv}$, and then $F_h = F_{yh}$):** The yielding sequence of the ties is in reverse.

5-   **Type E ($F_h < F_{yh}$, and $F_v < F_{yv}$):** It means the case where the concrete strut reaches its strength while the horizontal and vertical ties remain in the elastic range.

For type E, the equilibrium equations, presented before in section (2.3), are valid. For other analysis types, the equilibrium state under a given horizontal joint shear (Q_h) has to be modified after yielding. The parts of the joint shears beyond the yielding should be resisted by the reduced mechanisms. By setting $\gamma_h = 0$, the modified ratios of joint shear resisted by the diagonal and vertical mechanisms are recalculated during YH analysis. For YV analysis, the modified shear ratios of the diagonal and horizontal mechanisms are evaluated by assigning $\gamma_v = 0$. In [46], the details of the computational algorithms are presented for the force redistribution of the joint shears post the yielding of the horizontal and/or the vertical ties.

The proposed model is a statically indeterminate system. The yielding of ties does not stop the development of the shear strength because the inherent diagonal strut is capable of transferring the shear force alone. Failure is defined as the crushing of concrete in the compression strut adjacent to the nodal zone. Therefore, the shear strength of the joint is calculated as the concrete compressive stress on the nodal zone as it reaches its capacity. As shown in Figure (6), the boundary of the nodal zone coincides with the diagonal strut boundary, and the concrete bearing pressure to be examined at a node is the summation of compressive forces from the diagonal, flat, and steep struts. At failure, the maximum compressive stress ($\sigma_{d\,max}$) existing on the nodal zone in the d-direction is evaluated from resolution of compressive forces in Figure (6-b) as:

$$\sigma_{d\,max} = [\,D + B_1\,F_h + B_2\,F_v\,]\,/\,A_{strut} \tag{47}$$

$$B_1 = \cos\theta + 0.5\sin\theta\,\tan\theta \tag{48}$$

$$B_2 = \sin\theta + 0.5\cos\theta\,\cot\theta \tag{49}$$

3.2 **Solution procedure**

For implementing the proposed analytical model, a computer program was developed [46] for predicting the shear strength of exterior and interior joints. An incremental-iterative

solution technique was adopted in order to follow the material non-linearities of the steel and concrete in compression and tension and to activate the computational algorithms of the joint shears redistribution post the yielding of ties. The main algorithm starts with a selection of the horizontal joint shear (Q_h) and can be roughed out into three steps. The first step employs the forces equilibrium equations and yielding conditions of steel ties to find the maximum compressive stress in the diagonal strut ($\sigma_{d\ max}$) acting on the nodal zone. By assuming the strength of concrete strut is reached, a value of the softening coefficient (β) is obtained through ($\beta = \sigma_{d\ max} / f_c'$). Secondly, the constitutive laws are used to compute the strains of the struts and ties. The third step applies the compatibility conditions to compute new values of (β). If the assumed (β) is close enough to the computed (β) value, the (Q_h) selected is the shear strength of joint; otherwise back to iterations.

To not over estimate the softening effects in the situations where joint behavior is governed by yielding of all reinforcements crossing the crack direction, a limiting value of the strain (ε_r) is defined in calculating the coefficient (β). For the type YHV analysis, the value of (ε_r) corresponding to the point where the second yielded vertical tie is approaching the yield strain ($\varepsilon_v = \varepsilon_{yv}$) is computed as the limiting strain value. For the type YVH analysis, the (ε_r) limit can be calculated at the stage where (ε_h) is taken as (ε_{yh}) of the stirrups.

4. Experimental validation studies

4.1 Experimental verification for exterior and interior joints

The proposed model was used to predict the joint shear strength of 77 exterior test specimens (Table 1) and 55 interior test specimens (Table 2) described in the literature. These joints were tested by several researchers in Egypt, United States, New Zealand, Japan, Taiwan, United Kingdom, and Greece. The specimens selected encompass a wide range of material properties, geometry, loading sequence, reinforcement detailing, and failure modes. Only concentric specimens failing in a joint or a beam adjacent to a column were considered. Specimens failed prematurely in a column were omitted. The experimental joint shear strength ($Q_{h\ test}$) in Tables (1) and (2) were either reported in the literature or derived using equation (1) based on the maximum values of the beam and column shears, measured during the tests. According to the seismic performance of the beam-column subassemblages, the failure modes of beam-column specimens were classified [38,39] into F_1, J_1, J_2, and J_3 groups. The letter F designates the beam flexural failure, and the letter J indicates joint shear failure. The classification of F_1 and J_1 means that the joint strength can reach its design value after the yielding of sub-assemblage and the ductility is up to 4. Yielding of specimen occurred when the yielding moment was exceeded in both beams at the column face. The failure mode J_2 means that the yielding load precedes the joint shear failure (ductility ratio > 1), and the above sequence J_3 is in reverse.

In Table (1) and in Figure (10), satisfactory results were obtained from the comparison of measured and computed shear strengths of 77 exterior joint tests. The strength ratios, that are defined as the ratio of the measured to the calculated strength, indicate the precision of the proposed model. Also, examination of the tested and computed strengths of 55 specimens in Table (2) and Figure (11) indicate that the proposed model is capable of predicting the shear

strengths of the interior beam-column joints. The study of results listed in Table (1), Table (2), Figure (10), and Figure (11) highlights the following findings:

1-   For exterior joints, the average strength ratio is (1.06) and the standard deviation is (0.208). The corresponding values for interior joints are respectively (1.18) and (0.283). The higher strength ratio for interior joint is attributed to the better end conditions of its diagonal strut provided by the compression zone in beams and columns. This finding agrees with the nominal shear strength recommendations of ACI for different conditions of joint confinement provided by the framing beams.

2-   Despite the difference in test specimens, the proposed model predicts their shear strengths reasonably well. Data cover a broad spectrum of joints including variations in concrete strength ($20 \leq f_c^{'} \leq 42.9$ MPa), steel yield stress ($224 \leq f_y \leq 644$ MPa), joint shapes ($33 \leq \theta \leq 68$ deg.), joint shear capacities ($33.2 \leq Q_h \leq 1948$ kN), strut area ($43.38 \leq A_{strut} \leq 1302$ cm^2), and tie area ($0.0 \leq A_{tie} \leq 3096$ mm^2).

3-   The model yields reasonable estimations for seismically insufficient joint which were not detailed with the joint hoops nor the intermediate column bars ($A_{th} = A_{tv} = 0.0$). Also, conservative but reasonable predictions have been obtained for the specimens with inclined bars as tested by Tsonos et al [11] and Hakim [16]. This indicates the possible application of the model in the seismic evaluation for retrofits.

4-   Through the results of the present study, it is demonstrated that the seismic behavior of beam-column joints is sensitive to reduction of axial column compression; more so for tension applications.

4.2 <u>Overall statistical evaluation of analytical results</u>

In Table (3), the accuracy of the proposed model under varied conditions is further examined. The overall statistical evaluation of analytical results of exterior and interior joints in Table (3) reveals the following points:

1-   Compared with the previous analytical results [38,39], the shear prediction strength and failure mode are better for the proposed model. The average shear strength ratio is (1.11) and the standard deviation is (0.25). The corresponding values in [38,39] are respectively (1.21) and (0.27). The proposed model considers the progressive deterioration of a joint due to the accumulated concrete damage and steel yielding.

2-   The shear strength is well predicted for the specimens failing in joints. Better precision was obtained for the estimations of groups J_1 and J_2 with type E (SD = 0.16), but there was wider dispersion for group F_1 specimens. The lower degree of correlation for group F_1 (SD = 0.24) is consistent with its lower strength ratio (Avg. = 1.01). The reason is that the maximum stress was dictated mainly by the beam flexural strength and not necessarily by joint strength for F_1 specimens.

3-   Considering the specimens with J_1 failure mode, the shear strength ratio for type E is large, the values for type YH and YV are medium, and the ratio of type YHV and YVH are smaller. The occurrence of more yielding mechanisms leads to great damage

accumulation within the joint and consequently, less joint strength is expected. The occurrence of YV, YVH, and YHV failure types are not generally common for joints.

4-   The proposed model may over-predict the results for group J_3 specimens. This observation is attributed to the non-ductile response of the sub-assemblages (ductility ratio < 1) where the joint shear failure precedes the yielding of beam bars. Consequently, the estimation of diagonal strut depth using the compression zone depth in the column only may be small for J_3 cases.

5. <u>Parametric studies of joint shear resistance</u>

The strength behavior of the beam-column joints under seismic actions is very complicated. The sensitivities of the related parameters are still not clear. The proposed model maintains consistency in its estimations from one situation to another. Therefore, the proposed model herein was used to perform extensive studies to clarify the roles of different parameters in the seismic shear resistance of joints. The standard specimen for the parametric studies is shown in Figure (12) as given in [27]. The basic data is given as $f_c' = 27.4$ MPa, $f_{yh} = 414$ MPa, $f_{yv} = 448$ MPa, $\theta = 45$ deg., $A_{strut} = 194$ cm^2, $A_{th} = 190$ mm^2, and $A_{tv} = 774$ mm^2.

5.1 <u>Study of joint reinforcement parameters</u>

The effect of horizontal steel ratio and type on the normalized joint shear strength (q_h/f_c') is studied in Figure (13). Two case studies were analyzed as C_1 and C_2 for which the yield stress of hoops was 240 and 360 MPa respectively. It can be deduced from the figure that the joint shear strength increases with the increase of horizontal reinforcement ratio (ρ_h) and/or yield stress of steel. In enhancing the shear strength, the increase of (ρ_h) is more effective than increasing the yield stress. In comparison with the result at $\rho_h = 0\%$, the strength increase factor of 34% for case C_1 and 46% for case C_2 is achieved at $\rho_h = 2\%$. At $\rho_h = 1\%$, the increase of yield stress from 240 to 360 MPa leads to strength increase by 5% only. Numerous experiments have shown, hoop yield to be a critical factor in response as it makes a joint susceptible to cyclic deterioration [37]. The predictions made herein, indicated that the minimum steel ratio to prevent hoop yield is 0.6% for case C_1 and 0.4% for case C_2. In other words, the minimum hoop ratio ($\rho_{h\ min}$) is ($144/f_y$) in MPa units. Joint hoops carry a substantial portion of the joint shear, with the remainder being carried by the diagonal concrete strut. Also, the horizontal steel confines the concrete core, thereby increasing its compressive resistance of the strut and preserving the integrity of the connection.

In Figure (14), the influence of vertical steel ratio and type on the normalized joint shear strength is presented. Two case studies were considered as C_3 and C_4 for which the yield stress of intermediate column bars was 360 and 400 MPa respectively. It is clear that the higher the vertical steel ratio (ρ_v), the bigger is the joint strength. The increase of ρ_v from 0% to 1% leads to strength increase by 18%. Practically, the yield stress level of vertical steel has no effect on the joint horizontal resistance. The minimum vertical steel ratio to prevent the yield of column intermediate bars was found to be 0.3%.

In Figure (15), the effect of joint hoops distribution pattern on the normalized joint shear strength is illustrated. Three case studies were conducted as C_5, C_6, and C_7 for which

the total number of hoop layers is 3, 4, and 5 layers respectively. These layers were uniformly distributed along the constant joint depth. As shown, the use of closely spaced stirrups enhances the joint shear strength. The rate of strength improvement increases with the increase of stirrups area and hoop layers number. The strength improvement is due to the increase of effective area of the horizontal tie and confinement condition of concrete within the joint core. Due to the increase of $A_{stirrup}$ from 0 to 1000 mm^2, the shear strength increases by 26.3% for case C_5, 29.4% for case C_6, and 31.2% for case C_7. Relative to case C_5, the shear strength is higher by 2.4% for case C_6, and by 3.9% for case C_7 at $A_{stirrup} = 1000$ mm^2.

In the Figure (16), the effect of presence of additional cross inclined bars in the joint core on the normalized joint shear strength is presented. Three case studies were considered as C_8, C_9, and C_{10} for which the ratio of inclined bars is zero, 0.3%, 0.6% respectively. It is clear that, the use of cross-inclined bars improves considerably the performance of joints in shear. The joint shear strength increases with the increase of inclined reinforcement ratio, especially for small percentage of confining hoops. Compared with case C_8, the shear strength at $\rho_h = 0.4$% is higher by 7.5% for case C_9, and by 13.8% for case C_{10}. The corresponding strength increase at $\rho_h = 2$% is 2.7% for case C_9, and by 4.8% for case C_{10}. Also, the existence of inclined bars in lightly reinforced joints converts the YH failure mode of joint to E type. The predicted results indicate that the inclined bars and stirrups can be provided together as shear reinforcement to resist the shear forces in order to avoid the congestion of steel in joints.

During sever cyclic loading caused by earthquake actions, the slippage of longitudinal beam bars passing through interior beam-column joint may occur. In Figure (17), the effect of bond slip on the normalized shear strength of an interior connection is considered for three case studies as C_{11}, C_{12}, and C_{13}. The associated bond loss condition for these cases is zero, 50%, and 100% respectively. As expected, the bond loss leads to joint shear strength degradation, and may convert the joint failure mode from E type to YH or YV type. Compared with case C_{11}, the shear strength at $\rho_h = 0.4$% is less by 3% for case C_{12}, and by 12.8% for case C_{13}. The corresponding strength decrease at $\rho_h = 2$% is 4% for both cases. In the proposed model, the bond loss condition impairs the development of the shear resistance mechanism of the vertical ties.

5.2 Study of concrete parameters

The relation between the maximum shear stress at the instant of connection failure q_h, the concrete compressive strength, and the concrete confinement factor ($\rho_s f_{yh}/f_c'$ %) is shown in Figure (18). For unconfined concrete, one case study was considered as C_{14}. For confined concrete, two case studies were performed as C_{15} and C_{16}, for which the confinement factor was 15% and 30% respectively. It is evident that, for different confinement ratios, the higher strength specimens have higher joint shear capacity than that of lower strength ones. For case C_{14}, the ultimate shear resistance of specimen with $f_c' = 60$ MPa is 2.27 times the resistance of the specimen with $f_c' = 20$ MPa. For cases C_{15} and C_{16}, the corresponding average increase factor in joint shear strength is 2.23. The significant improvement in shear strength is mainly attributed to the resistance increase of inclined compression strut. The figure also shows that, for normal and high strength concrete, the increase of confinement factor enhances the joint shear strength. Compared with case C_{14}, the average increase in shear strength due to concrete

confinement is 14% for case C_{15} and 27% for case C_{16}. By converting the joint failure mode from YH type to E type, it was found that the increase of confinement factor prevents the yield of joint stirrups for different concrete grades.

5.3 Study of joint geometry parameters

In the proposed model, the distribution ratios of the joint shears resisted by the diagonal, horizontal, and vertical mechanisms are mainly affected by the inclination angle of concrete strut. Before yielding of horizontal and vertical ties, Figure (19) illustrates the effect of diagonal strut angle on the ratios of the joint shear resisting mechanisms. When the angle of inclination $\theta = 45$ deg, the diagonal mechanism carries the largest shear of the joint forces ($R_d = 0.5$) and the corresponding values of R_h and R_v are equal ($R_h = R_v = 0.25$). The figure indicates that the joint shear capacity is mainly controlled by the joint hoop resistance for $\theta > 45$ deg, and by the intermediate column bars resistance for $\theta < 45$ deg. The horizontal joint shear is entirely carried by the indirect load path of the horizontal mechanism for $\theta \geq \tan^{-1}$ (2), and is fully resisted by the vertical tie for $\theta \leq \tan^{-1}$ (1/2). If the vertical tie is absent or yielding, the entire horizontal shear is transferred by the direct compression strut for $\theta \leq \tan^{-1}$ (1/2). Also, if the horizontal tie is absent or yielding, the entire horizontal shear is carried by the concrete strut for $\theta \geq \tan^{-1}$ (2).

In Figure (20), the combined effect of the area and inclination angle of the concrete strut on the normalized joint shear resistance is presented. Three case studies were studied as C_{17}, C_{18}, and C_{19} for which the inclination angle θ is 30, 45, and 60 deg respectively. It is clear that the higher the strut area, the higher is the joint shear strength. The increase of strut area (A_{strut}) from 50 cm^2 to 250 cm^2 leads to strength increase by 343% for C_{17}, by 331% for C_{18}, and by 254% for C_{19}. The increase rate of shear strength is significantly higher for the smaller values of strut angle. At $A_{strut} = 200$ cm^2, the normalized shear strength is 0.2356 for C_{17}, 0.1437 for C_{18}, and 0.1008 for C_{19}. The predicted results confirm the fact that a substantial portion of the joint shear is carried by the diagonal strut for which the resistance is directly proportional to the cosine of inclination angle. For $\theta = 30$ and 45 deg, the predicted joint failure mode was E type at different values of A_{strut}. For $\theta = 60$ deg, the predicted failure mode converts to YH type where the horizontal tie yields before concrete crushing.

A critical aspect of inelastic seismic response of frame structure is the dimensional limitations of frame members to assure the strong column-weak beam behavior. The ACI provisions [31] state that the design flexural capacity of column at a joint should not be less than 1.2 times the design flexural capacity of the beam at that joint. However, no specific rules for the joint aspect ratio are currently given in design codes. In Figure (21), the effect of the joint aspect ratio on the horizontal joint shear strength is studied using different values of (beam thickness/column thickness) or (t_b/t_c) ratio. Three case studies were analyzed as C_{20}, C_{21}, and C_{22} for which the (beam width/column width) or (b_b/b_c) ratio was 0.25, 0.5, and 1.0 respectively. As shown in the figure, the joint shear capacity decreases significantly with the increase of (t_b/t_c) ratio. The increase of (b_b/b_c) ratio has practically no effect on the joint shear strength. The increase of (t_b/t_c) from 0.5 to 2 results in average decrease of shear capacity by 68% for the three cases. At (t_b/t_c) =1.0, the predicted joint shear capacity is 178.2 kN for C_{20},

207.5 kN for C_{21}, and 263.4 kN for C_{22} case. The increase of (t_b/t_c) ratio beyond 1.0 converts the predicted failure mode from E type to YH type. The detrimental effect of (t_b/t_c) ratio increase is explained using the following reasons:

1-   For constant value of column thickness (t_c), the increase of (t_b/t_c) ratio increases the strut inclination angle which decreases the contribution of the main shear resisting mechanism associated with the concrete diagonal strut.

2-   The depth of concrete strut increases with the increase of column thickness. Also, the increase of (b_b/b_c) ratio increases the effective width of concrete strut, and relieves the congestion of steel reinforcement within the joint core.

       Beam stubs at exterior joints provide improved anchorage of beam and column bars, and prevent the spalling of concrete cover of the column exterior face. These problems are practically acute when relatively small columns are used. In Figure (22), the effect of beam stub on the normalized shear strength of exterior joint is presented. Two joints are analyzed as C_{23} and C_{24} respectively without and with beam stub. As shown, the existence of beam stub increases the shear strength of the exterior joint, especially for relatively small concrete strut areas. At $A_{strut} = 250$ cm^2, the shear strength of C_{24} is higher by 13.5% than that of case C_{23}. The inclination angle of concrete strut is 48 and 45 degree respectively for C_{23} and C_{24}. Consequently, the presence of beam stub at exterior joint decreases the inclination of the diagonal strut and hence increases the concrete contribution of the diagonal shear resisting mechanism. Moreover, the prevention of concrete core spalling maintains the effective joint area.

5.4 <u>Study of column load parameters</u>

       The load type of framing columns is frequently compression. However, the load type may be a tension force as a consequence of overturning seismic moment coexisting with vertical component of earthquake ground motion. The effect of column load level and type on the normalized joint shear strength is presented in Figure (23). For different levels of column load ratio ($N / A_g f_c'$), two case studies were analyzed here as C_{25} and C_{26} for which the load type was compression and tension respectively. It is demonstrated that the seismic behavior of a beam-column joint is sensitive to the reduction of axial column compression, more so for tension applications. The vulnerability of joint performance was manifested in losses of shear strength due to the introduction of a tensile axial force or the absence of column compression. The beneficial effect of the axial compression is to increase the depth and capacity of the diagonal concrete strut. A shear strength increase of 79% was predicted due to the introduction of a compression load of 25% of the ultimate column strength. However, the high compression load in the column was reported [37] to accelerate the deterioration of the joint shear resisting mechanism as it converts the joint failure mode from type E to YH mode. The detrimental effect of the column tension load increases with the increase of the applied tension force. Under constant conditions of geometry and reinforcement, the study predicts zero joint shear strength due to the application of a tensile load of 25% of the column squash capacity.

6. <u>Conclusions</u>

Based on the results of the validation and parametric studies of the proposed nonlinear softened strut-and-tie model for the seismic shear resistance of reinforced concrete beam-column joints, the following conclusions are made:

1- The proposed nonlinear model has proved to be suitable for predicting the joint shear strength and failure modes of beam-column connections. From 30 source of literature, the model was found to reproduce the results of 77 exterior test specimens and 55 interior ones with good accuracy. The verification studies covered a broad spectrum of joints including variations in concrete strength, steel yield stress, joint shapes and sizes, concrete strut areas, reinforcement ratios and arrangements, and column load conditions. The proposed model can provide valuable insights into the seismic behavior and retrofitting of joints.

2- Shear behavior of connections is significantly dependent on joint reinforcement parameters. Higher ratios of joint hoops or intermediate column bars cause a remarkable increase in shear strength. The rate of strength improvement increases with the increase of the effective number of hoop layers along the joint depth, and decreases with the bond loss of beam bars within the joint core. To prevent yielding, the minimum joint hoop ratio is found to be $(144/f_y)$ in MPa. The cross inclined bars and stirrups can be provided together as shear reinforcement to avoid the steel congestion in joints. Practically, the yield level of vertical steel has no effect on joint resistance.

3- The joint geometry parameters have dominant effects on the failure modes and distribution ratios of the internal shear resisting mechanisms. A substantial portion of the joint shear is carried by the diagonal concrete strut for which the resistance increases with its area increase and its inclination (θ) decrease. For $\theta = 45$ deg, the diagonal strut carries the largest portion of joint shear. The shear capacity is mainly controlled by the hoop resistance for $\theta > 45$ deg, and by the vertical steel resistance for $\theta < 45$ deg. The increase of (beam thickness/column thickness) or (t_b/t_c) ratio decreases significantly the joint capacity. Early yielding of joint hoops occurs for $(t_b/t_c) > 1.0$, and $\theta \geq 60$ deg. For exterior joints, the existence of beam stub increases the shear strength, especially for relatively small column dimensions.

4- The seismic behavior of beam-column joint is considerably sensitive to concrete and column load parameters. For different confinement ratios, the higher strength specimens have higher joint shear capacity than that of lower strength ones. The increase of concrete confinement factor increases remarkably the shear strength and prevents the yielding of joint stirrups for different concrete grades. The vulnerability of joint performance is manifested in losses of shear strength due to the reduction of column compression load, or tension force applications. A shear strength increase of 79% was predicted due to the introduction of a compression load of 25% of the ultimate column capacity. A zero joint strength was predicted due to the application of a tensile load of similar magnitude.

References

1. Meggat, L.M., "Cyclic Behavior of Exterior Reinforced Concrete Beam-Column Joints", Bulletin of New Zealand National Society for Earthquake Eng., V.7, No.1,1974, pp.22-47.

2.   Lee, D.L.N.; Wight, J.K.; and Hanson, RD., "RC Beam-Column Joints under Large Load Reversals", J. Struct Div., ASCE Proc., V.103, No. 12, 1977, pp. 2337-2350.

3.   Pauly, T., and Scarpas, A., "Behavior of Exterior Beam-Column Joints", Bulletin of New Zealand National Society for Earthquake Eng., V. 14, No. 3, 1981, pp. 131-144.

4.   Park, R., and Milburn, J. R., "Comparison of Recent New Zealand and United States Seismic Design Provisions for Reinforced Concrete Beam-Column Joints and Tests Results from Four Units Designed According to the New Zealand Code", Bulletin of New Zealand National Society for Earthquake Eng., V. 16, No. 1, 1983, pp. 3-24.

5.   Kanada, K.; Kondon, G.; Fujii, S.; and Morita, S., "Relation Between Beam Bar Anchorage and Shear Resistance at Exterior Beam-Column Joints", Transaction of Japan Concrete Institute, V. 6, 1984, pp. 433-440.

6.   Ehsani, M. R., and Wight, J.K., "Exterior Reinforced Concrete Beam-to-Column Connections Subjected to Earthquake-Type Loading", ACI J., Proc. V. 82, No. 4, 1985, pp. 492-499.

7.   Zebra, H. E., and Durrani, A. J., "Effect of Slab on Behavior of Exterior Beam-to-Column Connections", Report No. 30, Rice University, Houston, Tex., 1985.

8.   Ehsani, M. R.; Moussa, A. E., and Vallenilla, C. R., "Comparison of Inelastic Behavior of Reinforced Ordinary and High-strength Concrete Frames", ACI Struct. J., V. 84, No. 2, 1987, pp. 161-169.

9.   Alameddine, F. F., " Seismic Design Recommendation for High Strength Concrete Beam-to-Column Connections", Ph.D. thesis, University of Arizona, 1990.

10.   Fujii, S., and Morita, S., "Comparison between Interior and Exterior RC Beam-Column Joint Behavior", SP-123, ACI, 1991, pp.145-165.

11.   Tsonos, A. G., Tegos, I. A., and Penelis, G. Gr., " Seismic Resistance of Type 2 Exterior Beam-Column Joints Reinforced with Inclined Bars", ACI Struct. J., V. 89, No. 1, 1992, pp. 3-12.

12.   Kaku, T., and Asakusa, H., "Ductility Estimation of Exterior Beam-Column Subassemblages in Reinforced Concrete Frames", SP-123, ACI, 1991, pp.167-185.

13.   Hwang, S. J., and Lin, M. S., "Evaluation of Seismic Behavior of Corner Beam-Column Joints Using High Performance Concrete (I)", National Science Council Project Report, No. NSC 85-2211-E-011-004, Taiwan, 1996.

14.   Hwang, S. J., and Chen, C. S., "Evaluation of Seismic Behavior of Corner Beam-Column Joints Using High Performance Concrete (II)", National Science Council Project Report, No. NSC 86-2211-E-011-014, Taiwan, 1997.

15.   Abdel-Hadi, S. A. A., "Experimental and Analytical Study of Exterior R/C Beam Column Connections", Ph.D. thesis, Faculty of Engineering, Cairo University, 1998.

16.   Hakim, T. M., "Inelastic Behavior of Reinforced Concrete Joints", Ph.D. thesis, Faculty of Engineering, Ain-Shams University, 2000.

17.   Meinheit, D. F., and Jirsa J. O., "The Shear Strength of Reinforced Concrete Beam-Column Joints", CESRL Report No. 77-1, University of Texas at Austin, 1977.

18.   Fenwick, R. C., and Irvine, H. M., "Reinforced Concrete Beam-Column Joints for Seismic Loading", School of Engineering Report No.142, University of Auckland, New Zealand, 1977.

19.   Birss, G.R., "The Elastic Behavior of Earthquake Resistant Reinforced Concrete Beam-Column Joints", Research Report No.78-13, University of Canterbury, New Zealand, 1978.

20.   Beckingsale, C. W., "Post-Elastic Behavior of Reinforced Concrete Beam-Column Joints", Research Report No. 80-20, University of Canterbury, New Zealand, 1980.

21.   Park, R., Gearty, L., and Stevenson, E. C., "Tests on an Interior Reinforced Concrete Beam-Column Joint", Bulletin of New Zealand National Society for Earthquake Eng., V.14, No. 2, 1981, pp. 81-92.

22.   Durrani, A. J., and Wight, J. K., "Behavior of Interior Beam-to-Column Connections Under Earthquake-Type Loading", ACI J., Proc. V. 82, No. 3, 1985, pp. 343-349.

23.   Otani, S., Kobayshi, Y., and Aoyama, H., "Reinforced Concrete Interior Beam-Column Joints Under Simulated Earthquake Loading", First U.S.-N.Z.-Japan Seminar, Monterey, 1984.

24.   Otani, S., Kitayama, K., and Aoyama, H., "Beam Bar Bond Stress and Behavior of Reinforced Concrete Interior Beam-Column Connections", Second U.S.-N.Z.-Japan Seminar, Tokyo, 1985.

25.   Abrams, D. P., "Scale Relations for Reinforced Concrete Beam-Column Joints," ACI Struct. J., V. 84, No. 6, 1987, pp. 502-512.

26.   Noguchi, H., and Kurusu, K., "The Effects of Beam Bar Bond and Joint Shear on the Behavior of Reinforced Concrete Interior Beam-to-Column Joints", Third U.S.-N.Z.-Japan Seminar, Christchurch, 1987.

27.   Leon, R. T., "Shear Strength and Hysteretic Behavior of Interior Beam-Column Joints", ACI Struct. J., V. 87, No. 1, 1990, pp. 3-11

28.   Higazy, E. M., Elnashai, A. S., and Agbabian, M. S., "Behavior of Beam-Column Connections Under Axial Column Tension", J. Struct. Eng., ASCE, V. 122, No.5, 1996, pp. 501-511.

29.   Joh, O., Goto, Y., and Shibata, T., "Influence of Transverse Joint and Beam Reinforcement and Relocating of Plastic Hinge Region on Beam-Column Joint Stiffness Deterioration", SP-123, ACI, 1991, pp. 187-224.

30. Kitayama, K., Otani, S., and Aoyama, H., "Development of Design Criteria for RC Interior Beam-Column Joints", SP-123, ACI, 1991, pp. 97-123.

31. ACI Committee 318, "Building Code Requirement for Structural Concrete (ACI 318-95) and Commentary (318R-95)", American Concrete Institute, Mich., 1995.

32. Architecture Institute of Japan, Design Guidelines for Earthquake Reinforced Concrete Buildings Based on Ultimate Strength Concept and Commentary, 1990.

33. NZS 3101:1995, Concrete Structures Standard, NZS 3101: Part 1, Commentary NZS 3101: Part 2, Standards Association of New Zealand, Wellington, 1995.

34. "Egyptian Code of Practice for Design of Reinforced Concrete Structures", ECCS203-2100, 7th ed., Egypt, 2001.

35. Jirsa, J. O. (ed.), "Design of Beam-Column Joints for Seismic Resistance", SP-123, ACI, Mich., 1991.

36. ACI-ASCE committee 352, "Recommendations for Design Concrete Structures", ACI J., Proc. V.82, No. 3, May-June 1985, pp. 266-283.

37. Paulay, T., and Priestley, M. J. N., "Seismic Design of Reinforced Concrete and Masonry Buildings", John Wiley & Sons, 1992.

38. Hwang, S. J., and Lee, H. J., "Analytical Model for Predicting Shear Strengths of Exterior Reinforced Concrete Beam-Column Joints for Seismic Resistance", ACI Struct. J., V. 96, No. 5, 1999, pp. 846-857.

39. Hwang, S. J., and Lee, H. J., "Analytical Model for Predicting Shear Strengths of Interior Reinforced Concrete Beam-Column Joints for Seismic Resistance", ACI Struct. J., V. 97, No. 1, 2000, pp. 35-44.

40. Paulay, T., "Equilibrium Criteria for Reinforced Concrete Beam-Column Joints", ACI Struct. J., V. 86, No. 6, 1989, pp. 635-643.

41. Pantazopoulou, S., Bonacci, J., "Consideration of Questions about Beam-Column Joints", ACI Struct. J., V. 89, No. 1, 1992, pp. 27-36.

42. Schafer, K., "Strut-and-Tie Models for Design of Structural Concrete", Notes of Workshop, National Cheng Kung University, Taiwan, 1996.

43. Park, R. and Paulay, T., "Reinforced Concrete Structures", John Wiley & Sons, 1975.

44. Zhang, L. X. B., and Hsu, T. T. C., "Behavior and Analysis of Concrete Membrane Elements", J. Struct. Eng., ASCE, V. 124, No. 1, 1998, pp 24-34.

45. Gipata, A. K., and Maestrini, S. R., "Post-Cracking Behavior of Membrane Reinforced Concrete Elements Including Tension Stiffening", J. Struct. Eng., ASCE, V. 115, No. 4, 1989, pp 957-976.

46. Abd El-Maula, A. S., "Evaluation of Shear Strength of Reinforced Concrete Beam-Column Joints", M.Sc. Thesis to be Submitted, Faculty of Engineering, Shobra, Zagazig University, 2002.

serial	Authors	f_c' (Mpa)	f_{yh} (Mpa)	f_{yv} (Mpa)	q deg.	A_{strut} (cm²)	A_{th} (mm²)	A_{tv} (mm²)	N / $A_g f_c'$	Q_h test (kN)	S.F. mode	J.F. mode	Q_h calc. (kN)	Q_h test / Q_h calc.
1	Meggat [1]	22.1	317	365	53	389	1330	774	0.07	576	J1	E	423.6	1.36
2	Lee et al [2]	29.0	389	0	42	194	426	0	0.11	194	F1	YV	272.23	0.71
3		24.8	389	0	42	142	426	0	0.00	206	J1	YV	189.1	1.09
4		24.8	273	0	42	142	126	0	0.00	208	J1	YVH	155.02	1.34
5	Paulay et al [3]	22.6	326	296	55	616	1356	1256	0.05	754	J1	E	649.5	1.16
6		22.5	326	296	55	788	942	1256	0.15	990	J1	YH	710	1.39
7		26.9	316	296	55	616	628	1256	0.05	753	F1	YH	630	1.20
8	Park et al [4]	38.2	321	485	49	415	471	628	0.10	606	F1	YH	641	0.95
9	Kanada et al [5]	24.3	0	0	59	404	0	0	0.00	256	J3	YHV	282.43	0.91
10		26.7	294	0	59	225	256	0	0.00	339	J2	YVH	233.2	1.45
11		30.1	294	0	59	225	640	0	0.00	337	J2	YVH	297.1	1.13
12		26.7	0	0	59	225	0	0	0.00	188	J2	YHV	185.64	1.01
13		30.1	294	0	59	225	256	0	0.00	198	J2	YVH	259.6	0.76
14	Ehsani et al [6]	33.6	437	490	68	520	881	568	0.06	554	J3	YH	492.6	1.12
15		40.9	437	490	68	271	881	568	0.06	591	J2	YH	360.3	1.64
16		44.6	437	490	66	267	881	568	0.06	635	J1	YH	360.3	1.76
17		24.3	437	414	62	670	881	1019	0.13	571	J3	YH	571.95	1.00
18		39.8	437	490	62	354	881	568	0.07	469	J1	YH	507.6	0.92
19	Zebra et al [7]	39.4	531	483	57	271	516	1019	0.05	438	J2	YH	437.1	1.00
20		39.9	531	483	56	270	516	1019	0.05	449	F1	E	451.2	1.00
21	Ehsani et al [8]	64.7	455	455	58	307	881	568	0.02	486	F1	YH	623.15	0.78
22		67.3	455	455	58	332	881	568	0.04	609	J1	YH	666.7	0.91
23		64.7	455	455	60	275	881	568	0.07	542	J1	YH	552.6	0.98
24		67.3	455	455	60	266	881	774	0.05	627	J2	YH	550.8	1.14
25	Alameddine [9]	56.5	446	479	58	360	1191	774	0.04	860	J2	E	731.5	1.18
26		56.5	446	479	58	360	1935	774	0.04	838	J2	E	776	1.08
27		56.5	446	457	57	662	1161	1019	0.07	987	J3	YH	1144.8	0.86
28		56.5	446	457	57	392	1935	1019	0.07	986	J2	E	842.5	1.17
29		74.5	446	479	59	349	1161	774	0.03	769	J2	YH	761.15	1.01
30		74.5	446	479	59	347	1935	774	0.03	934	J1	E	848.5	1.10
31		74.5	446	457	59	644	1161	1019	0.06	967	J3	YH	1196	0.81
32		74.5	446	457	59	385	1935	1019	0.06	1021	J2	E	931	1.10
33		92.4	446	479	59	338	1161	774	0.02	878	J2	YH	804.7	1.09
34		92.4	446	479	58	337	1935	774	0.02	890	J2	E	910.5	0.98
35		92.4	446	457	57	360	1935	1019	0.04	1032	J2	E	971.5	1.06
36	Fujii et al [10]	30.0	291	387	51	223	112	508	0.07	246	J3	YH	266.2	0.92
37		30.0	291	387	51	149	112	508	0.07	214	J2	YH	187.4	1.14
38		30.0	291	387	51	274	112	508	0.24	273	J3	YH	317.75	0.86
39		30.0	291	387	51	274	336	508	0.24	287	J3	YH	341.62	0.84
40	Tsonos et al [11]	26.0	490	485	63.4	108.5	376	551	0.025	182.41	F1	E	145.8	1.25
41		24.0	490	485	63.4	106.12	376	551	0.018	125.41	F1	E	134.8	0.93
42		27.0	490	485	63.4	110.2	376	551	0.03	228.02	J1	E	152	1.50

Table (1) - Results of experimental verification for exterior joints

serial	Authors	f_c' (Mpa)	f_{yh} (Mpa)	f_{yv} (Mpa)	q deg.	A_{strut} (cm^2)	A_{th} (mm^2)	A_{tv} (mm^2)	$N / A_g f_c'$	Q_h test (kN)	S.F. mode	J.F. mode	Q_h calc. (kN)	Q_h test / Q_h calc.
43		31.1	250	0	48	192	168	0	0.17	249	F1	YVH	266.26	0.94
44		41.7	250	0	48	162	168	0	0.10	244	F1	YVH	299.6	0.81
45		41.7	250	0	48	121	168	0	0.00	212	J1	YVH	225.01	0.94
46		44.7	281	0	48	189	42	0	0.17	236	J1	YVH	347	0.68
47		36.7	281	0	48	158	42	0	0.09	220	J1	YVH	247.58	0.89
48		40.4	281	0	48	121	42	0	0.00	208	J1	YVH	208.9	1.00
49	Kaku et al	32.2	250	395	47	172	168	284	0.12	249	F1	YH	239.85	1.04
50	[12]	41.2	250	395	47	154	168	284	0.08	243	F1	YH	266.4	0.91
51		40.6	250	395	47	121	168	284	0.00	234	J1	YH	216.75	1.08
52		44.4	281	395	47	190	42	284	0.17	241	F1	YH	314.75	0.77
53		41.9	281	395	47	153	42	284	0.08	229	J1	YH	275.2	0.83
54		35.1	281	395	47	121	42	284	0.00	207	J1	YH	183.2	1.13
55		46.4	250	395	47	103	168	284	-0.04	207	J1	YH	203.1	1.02
56		41.0	281	282	47	154	42	128	0.08	224	J1	YHV	260.75	0.86
57		39.7	281	395	47	155	42	71	0.08	229	J1	YHV	233	0.98
58		37.4	250	381	47	121	168	508	0.00	250	F1	YH	214.95	1.16
59	Hwang et al	33.4	434	463	59	1075	1161	1290	0.00	1142	J3	YH	1194.6	0.96
60	[13]	33.4	434	463	49	1002	774	1290	0.00	1226	J3	YH	1358.5	0.90
61		70.0	476	448	47	576	1200	1638	0.00	1490	F1	E	1391.4	1.07
62	Hwang et al [14]	62.4	476	500	56	400	1200	1020	0.00	1092	J2	E	850.5	1.28
63		64.2	500	500	56	400	774	1020	0.00	1063	J2	YH	801.6	1.33
64		21.1	224.5	0	59.6	43.38	22.9	0	0.12	38.75	F1	YVH	35.15	1.10
65		21.1	224.5	0	59.6	43.38	0	0	0.12	36.53	F1	YHV	25.84	1.41
66		21.7	224.5	0	59.6	43.48	22.9	0	0.12	34.32	F1	YVH	36.15	0.95
67	Abdel-Hady	21.7	224.5	0	59.6	43.48	0	0	0.12	33.215	F1	YHV	26.616	1.25
68	[15]	23.2	318.3	0	59.6	44.14	22.9	0	0.126	40.95	F1	YVH	37.22	1.10
69		23.2	318.3	0	59.6	44.14	0	0	0.126	37.64	J1	YHV	28.91	1.30
70		22.6	318.3	0	59.6	44.23	22.9	0	0.127	37.64	F1	YVH	41.93	0.90
71		22.6	318.3	0	59.6	44.23	0	0	0.127	37.1	J1	YHV	28.26	1.31
72		20.2	249	0	48.8	125	100.53	0	0.00	104.65	J1	YVH	113.47	0.92
73		20.0	370	0	48.8	125	100.53	0	0.00	115.5	J1	YVH	104.22	1.11
74	Hakim [16]	20.8	249	241.2	48.8	125	201.06	402.12	0.00	144.41	F1	E	132.05	1.09
75		20.6	249	0	45	125	100.53	0	0.00	148	F1	YVH	117.11	1.26
76		20.0	249	0	48.8	187.5	100.53	0	0.00	140.7	J1	YVH	166.824	0.84
77		20.5	249	241.2	48.8	125	302.56	302.56	0.00	151.62	F1	E	141.05	1.07
													Average	1.0626
													S	0.2078

Table (1) (cont.) - Results of experimental verification for exterior joints

serial	Authors	f_c' (Mpa)	f_{yh} (Mpa)	f_{yv} (Mpa)	q deg	A_{strut} (cm²)	A_{th} (mm²)	A_{tv} (mm²)	N / $A_g f_c'$	Q_h test (kN)	S.F. mode	J.F. mode	Q_h calc. (kN)	Q_h test / Q_h calc.
1	Meinheit et al [17]	26.2	409	457	44	980	516	516	0.39	1090	J3	YH	1232.5	0.88
2		41.8	409	449	45	804	516	516	0.25	1597	J3	YH	1629	0.98
3		26.6	409	402	46	973	516	516	0.39	1228	J3	YH	1330.5	0.92
4		36.1	409	438	59	903	1032	1032	0.29	1454	J3	YH	1072.2	1.36
5		35.9	409	449	45	593	516	516	0.04	1530	J3	YH	1101.25	1.39
6		36.8	409	449	45	979	516	516	0.47	1646	J2	YH	1738.2	0.95
7		35.2	423	449	46	755	2000	2000	0.29	1948	J2	E	1387.2	1.40
8		41.3	409	449	45	808	1290	1290	0.25	1557	J3	E	1611	0.97
9		33.2	409	438	59	932	2580	2580	0.31	1539	J3	E	1382.4	1.11
10	Fenwick et al [18]	42.9	275	280	45	188	1533	1533	0.00	521	J1	E	397.8	1.31
11		39.3	275	318	47	188	1799	1799	0.00	437	J1	E	376.6	1.16
12	Birss [19]	27.9	346	427	55	617	1520	1520	0.05	1217	J2	E	804	1.51
13		31.5	398	427	55	1302	398	398	0.44	1213	J1	YH	1361	0.89
14	Beckingsale [20]	35.9	336	423	55	596	3096	3096	0.04	965	F1	E	1020	0.95
15		34.6	336	422	55	599	3096	3096	0.04	982	F1	E	993	0.99
16		31.4	336	398	55	976	2580	2580	0.26	1015	F1	E	1393	0.73
17	Park et al [21]	34.0	305	412	49	539	1608	628	0.24	966	J2	E	879	1.10
18	Park et al [4]	41.3	320	473	50	415	2413	905	0.10	1001	J1	E	814	1.23
19	Durrani et al [22]	34.3	352	414	51	388	881	1020	0.05	840	J2	E	619.25	1.36
20		33.6	352	414	51	389	881	1020	0.06	853	J1	E	610.5	1.40
21		31.0	352	345	51	386	881	568	0.05	629	J1	E	556.25	1.13
22	Otani et al [23]	25.6	367	374	45	284	128	762	0.08	516	J1	YH	359.6	1.43
23		24.0	367	374	45	288	256	762	0.08	536	J1	E	351.6	1.52
24		24.0	367	374	45	288	640	762	0.08	576	J1	E	378.4	1.52
25		25.7	367	374	45	400	128	762	0.28	503	J1	YH	483	1.04
26		28.7	367	374	45	277	128	0	0.07	491	J1	YVH	326.83	1.50
27		28.7	367	374	45	277	256	284	0.07	336	F1	E	368.4	0.91
28	Otani et al [24]	25.6	324	422	45	284	128	762	0.08	436	F1	YH	358.05	1.22
29		25.6	324	422	45	284	512	762	0.08	432	F1	E	385.6	1.12
30		25.6	324	422	45	284	512	762	0.08	410	F1	E	385.6	1.06
31	Abrams [25]	31.1	400	470	33	392	284	0	0.00	724	J1	YV	547.75	1.32
32		34.3	400	470	34	392	284	0	0.00	789	F1	YV	583.1	1.35
33	Noguchi et al [26]	32.9	330	348	45	271	64	762	0.06	553	J1	YH	419.1	1.32
34		32.9	330	348	45	271	64	762	0.06	623	J1	YH	419.1	1.49
35		28.5	330	348	45	278	640	762	0.07	570	F1	E	419.6	1.36
36		28.5	330	348	45	278	64	762	0.07	605	F1	YH	379.2	1.60
37	Leon [27]	30.3	414	448	52	161	190	774	0.00	358	J2	YH	216.1	1.66
38		27.4	414	448	45	194	190	774	0.00	394	J1	E	271.05	1.45
39		27.2	414	448	40	226	190	516	0.00	462	F1	E	344.4	1.34
40	Higazy et al [28]	28	360	0	50.2	51.71	126.67	0	-0.025	83.03	J1	YV	69.5	1.19
41		28	360	0	50.2	51.71	63.34	0	-0.025	80.08	J1	YVH	60.72	1.32
42		42	360	0	50.2	51.71	126.67	0	-0.025	84.47	J1	YVH	82.4	1.03

Table (2) - Results of experimental verification for interior joints

serial	Authors	f_c' (Mpa)	f_{yh} (Mpa)	f_{yv} (Mpa)	q deg	A_{strut} (cm^2)	A_{th} (mm^2)	A_{tv} (mm^2)	N / A_g f_c'	Q_h test (kN)	S.F. mode	J.F. mode	Q_h calc. (kN)	Q_h test / Q_h calc.
43		25.6	1320	404	50	342	400	762	0.15	272	F1	E	469.4	0.58
44		27.4	1320	404	50	335	400	762	0.14	277	F1	E	482.4	0.57
45	Joh et al [29]	28.1	377	404	50	332	280	762	0.14	275	F1	YH	406	0.68
46		26.9	377	404	50	337	168	762	0.15	274	F1	YH	382.4	0.72
47		26.1	377	404	50	340	280	0	0.15	239	F1	YVH	361.81	0.66
48		30.6	320	540	46	355	168	1194	0.06	689	J3	YH	518.5	1.33
49	Kitayama et al [30]	24.5	235	351	46	286	168	1194	0.08	570	J1	YH	349.5	1.63
50		24.5	235	351	46	286	168	1194	0.08	570	J2	YH	349.5	1.63
51		24.5	235	371	45	286	420	762	0.08	515	J1	E	363.2	1.42
52		40.2	291	644	51	223	112	762	0.08	412	J3	YH	353.85	1.16
53	Fujii et al [10]	40.2	291	387	51	223	112	762	0.08	380	J3	YH	353.85	1.07
54		40.2	291	644	51	269	112	762	0.23	412	J3	YH	417.2	0.99
55		40.2	291	644	51	269	336	762	0.23	421	J3	YH	440.4	0.96

Average	1.1796
S	0.2829

Table (2) (cont.) - Results of experimental verification for interior joints

J. F. mode	Subassemblage failure mode												TOTAL		
	F1			J1			J2			J3					
	No.	Ave.	S.D.	No.	Ave.	S.D.	No.	Ave.	S.D.	No.	Ave.	S.D.	No.	Ave.	S.D.
E	16	1.00	0.23	13	1.33	0.16	11	1.20	0.17	2	1.04	0.10	42	1.16	0.23
YH	11	1.00	0.28	15	1.19	0.29	10	1.26	0.28	19	1.02	0.18	55	1.10	0.27
YV	2	1.03	0.45	3	1.20	0.12	None			None			5	1.13	0.26
YHV	2	1.33	0.12	4	1.11	0.23	1	1.01	---	1	0.91	---	8	1.13	0.21
YVH	8	0.97	0.19	11	1.05	0.25	3	1.12	0.35	None			22	1.03	0.23
TOTAL	39	1.01	0.24	46	1.19	0.25	25	1.21	0.24	22	1.01	0.17	132	1.11	0.25

Table (3) - Statistical analysis of results of exterior and interior joints
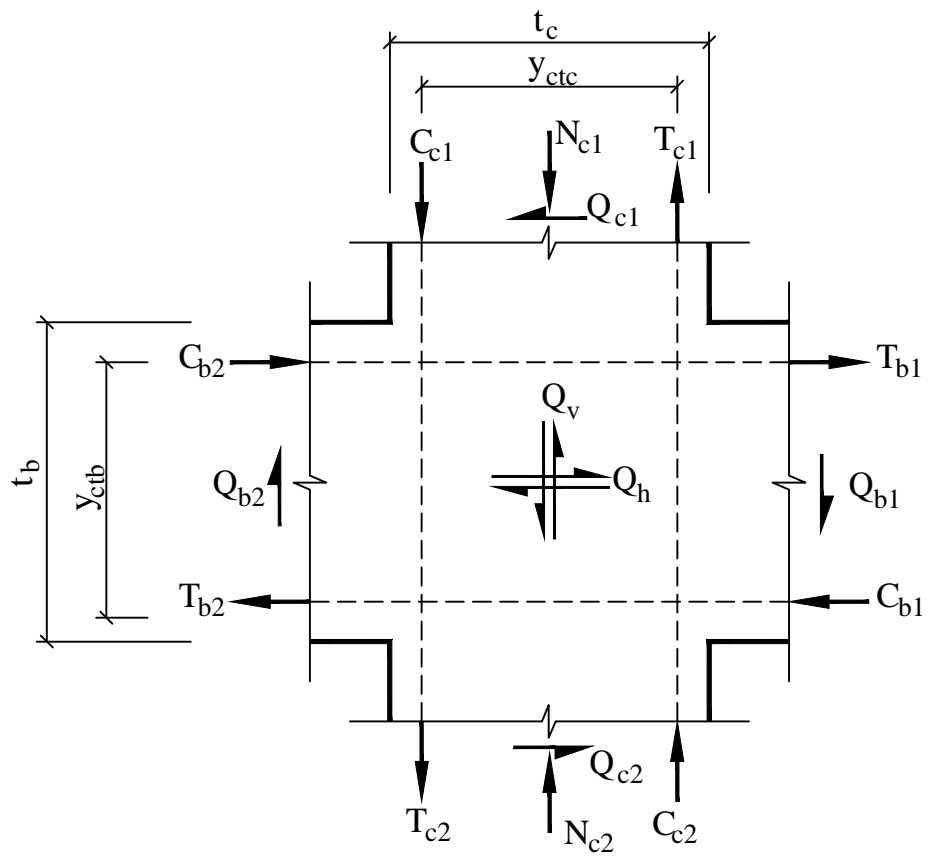
Fig. (1) - External actions and internal shears at beam-column joint
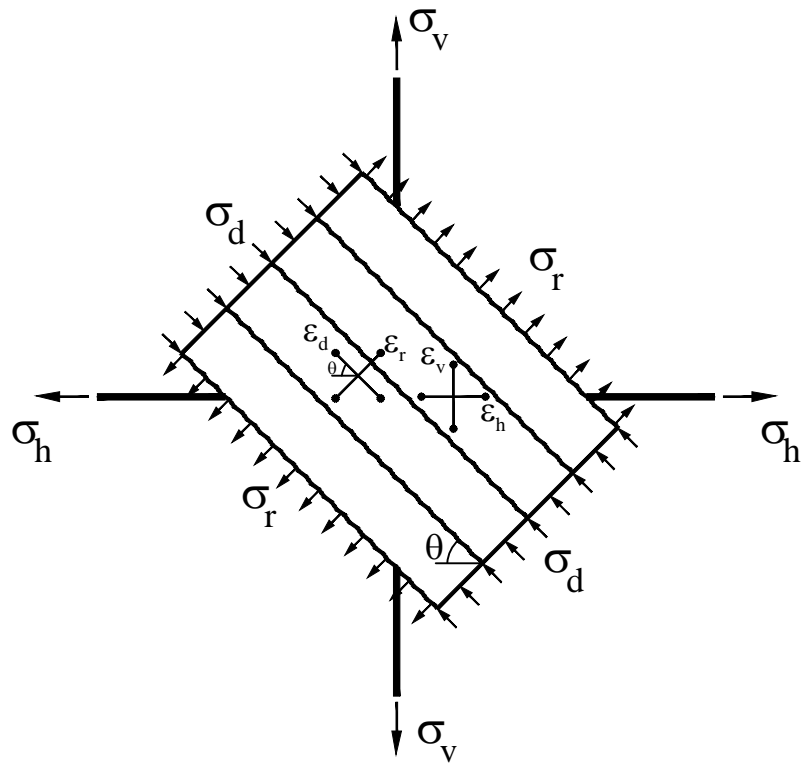
Fig.(2) - State of stress and strain in the cracked joint core

(3-a) Interior joint

(3-b) Exterior joint without beam stub

(3-c) Exterior joint with beam stub

Fig. (3) - Definition of compression strut [38,39]
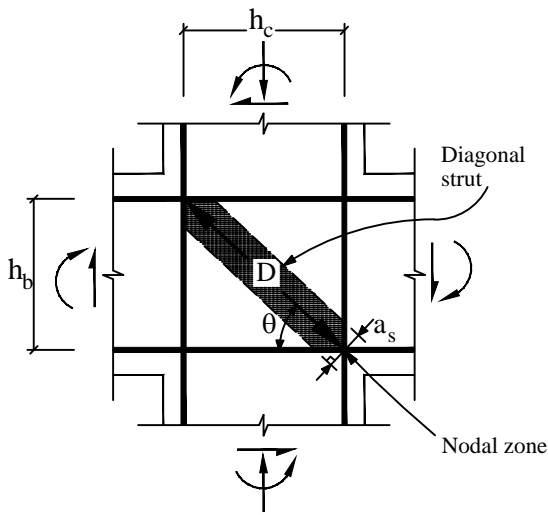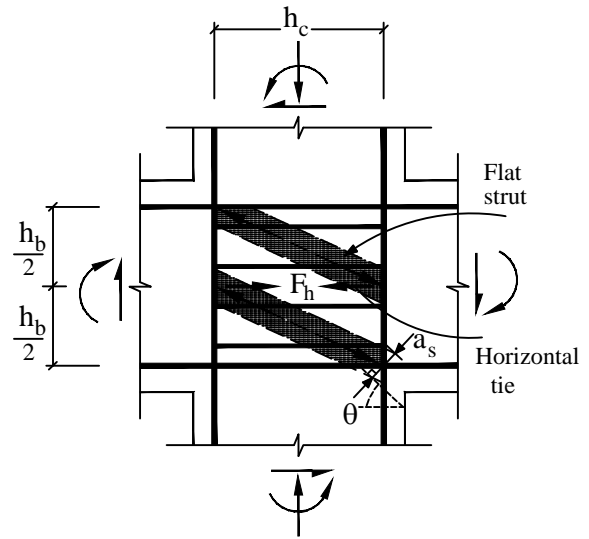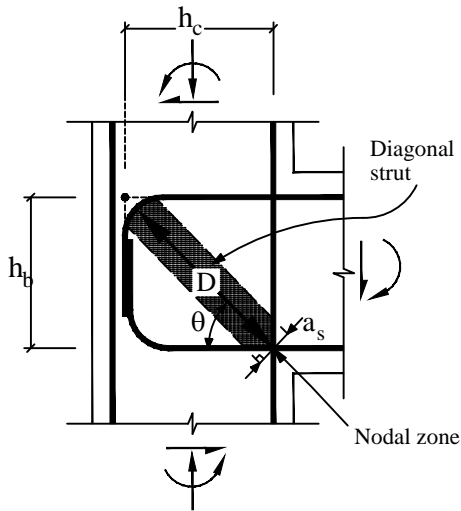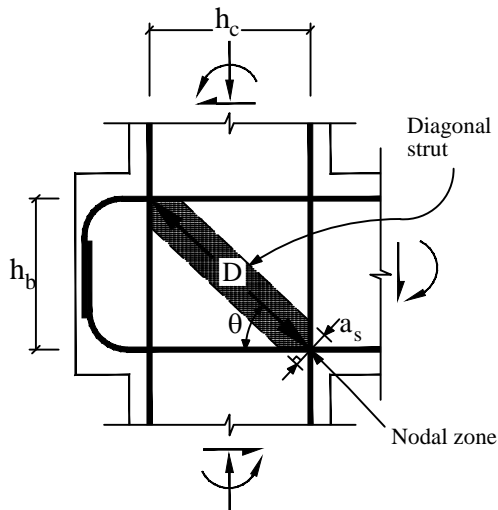
(4-a) Horizontal mechanism

(4-b) Vertical mechanism
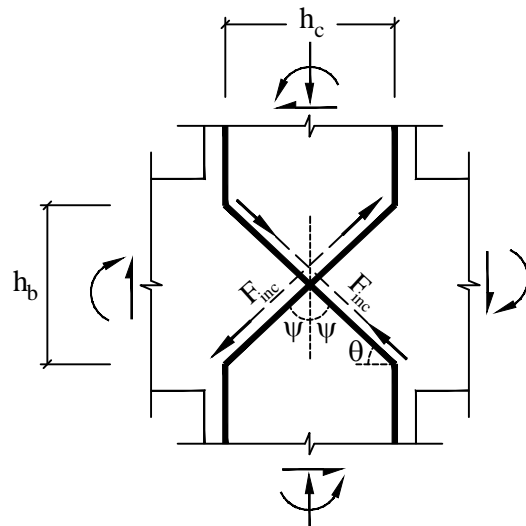
(4-c) Effect of inclined bars

Fig. (4) - Definition of horizontal and vertical mechanisms [11,39]

n_{th}	1	2	3	4	5	6	7	8
n_{eh}	1	2	2	3	4	5	5	6
n_{tv}	1	2	3	4	5	6	7	8
n_{ev}	1	2	3	3	4	5	6	6

$S_v \, S_v \, S_v \, S_v$

$\dfrac{S_h}{2}$ S_h S_h $\dfrac{S_h}{2}$

$n_{th} = 3$
$n_{eh} = 2$

$n_{tv} = 3$, $n_{ev} = 3$
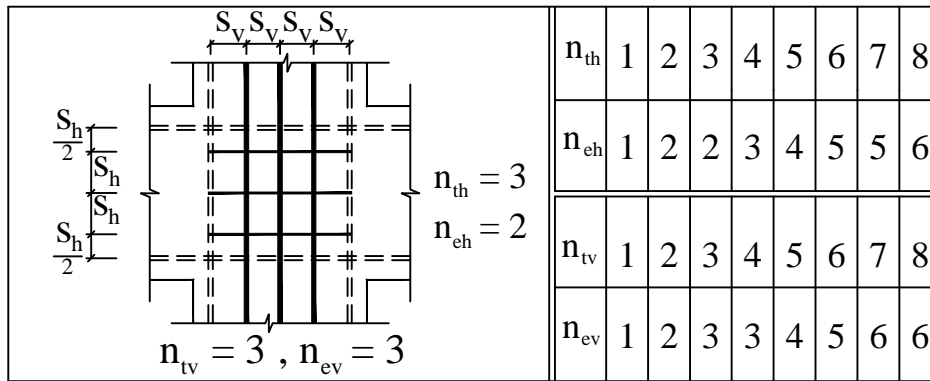
Fig. (5) - Determination of areas of horizontal and vertical ties

$\dfrac{Q_v}{2}$ $\dfrac{Q_h}{2}$ $\dfrac{Q_h}{2}$ F_v $\dfrac{Q_v}{2}$ F_h D

- - - - - Comp. strut

———— Tension tie

(6-a) Forces acting on joint region

$\dfrac{Q_v}{2}$ $\dfrac{Q_h}{2}$ $\dfrac{Q_h}{2}$ $D\sin\theta$ $\dfrac{F_h \tan\theta}{2}$ $D\cos\theta$ F_v F_h F_v $\dfrac{F_v \cot\theta}{2}$ F_v $\dfrac{F_v \cot\theta}{2}$ F_h θ $\dfrac{Q_v}{2}$ $\dfrac{F_h \tan\theta}{2}$ F_h
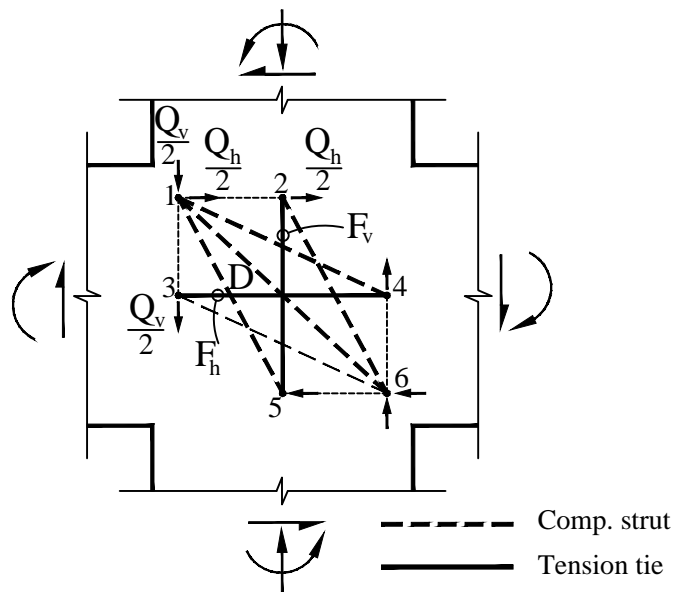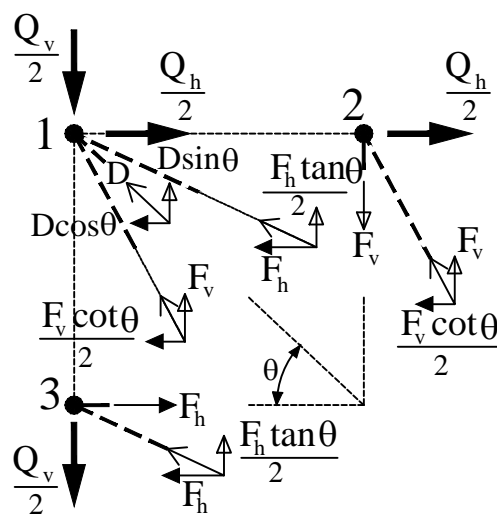
(6-b) Forces acting on nodes

Fig. (6) - Strut-and-tie model at maximum response
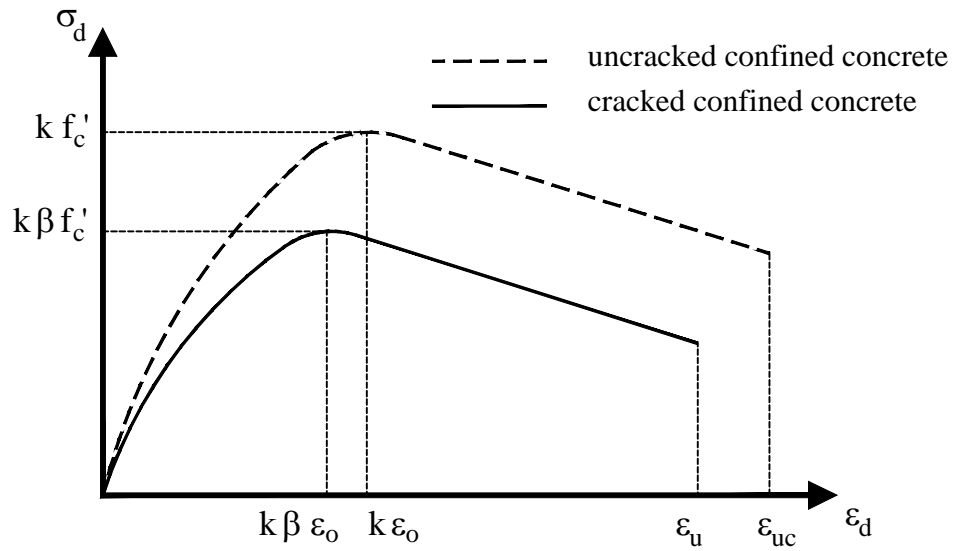
Fig. (7) - Constitutive compression law for concrete
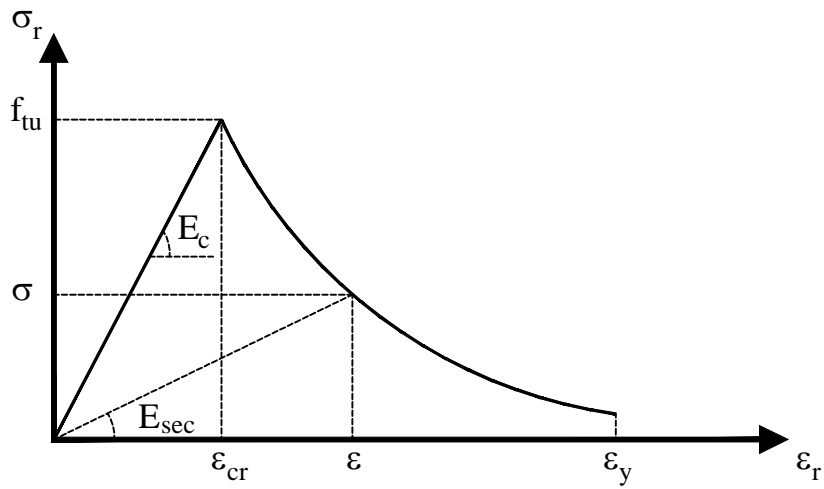
Fig. (8) - Concrete behavior in tension [44]
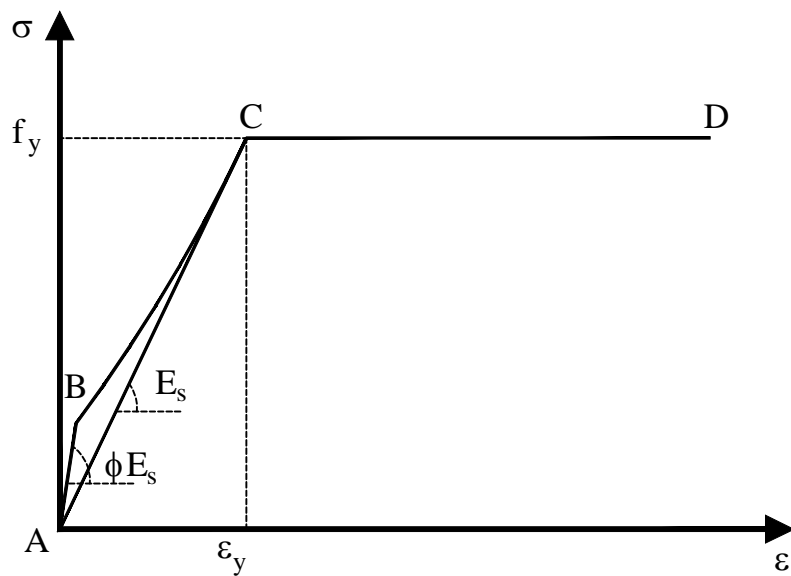
Fig. (9) - Constitutive law of steel including tension stiffning
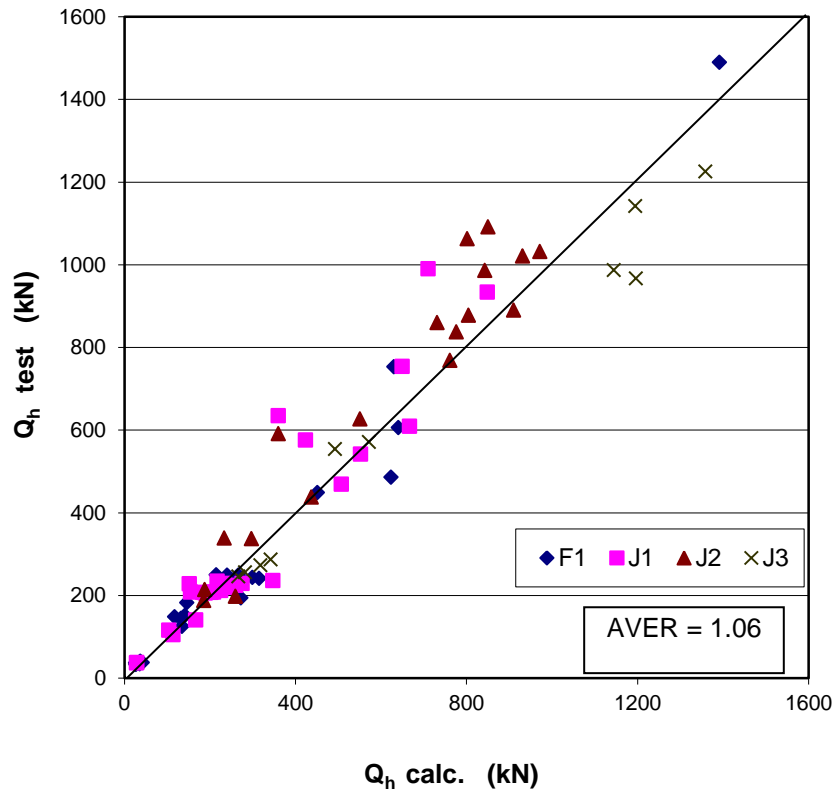
Fig.(10)- Correlation of experimental and predicted joint shear strengths for exterior joints
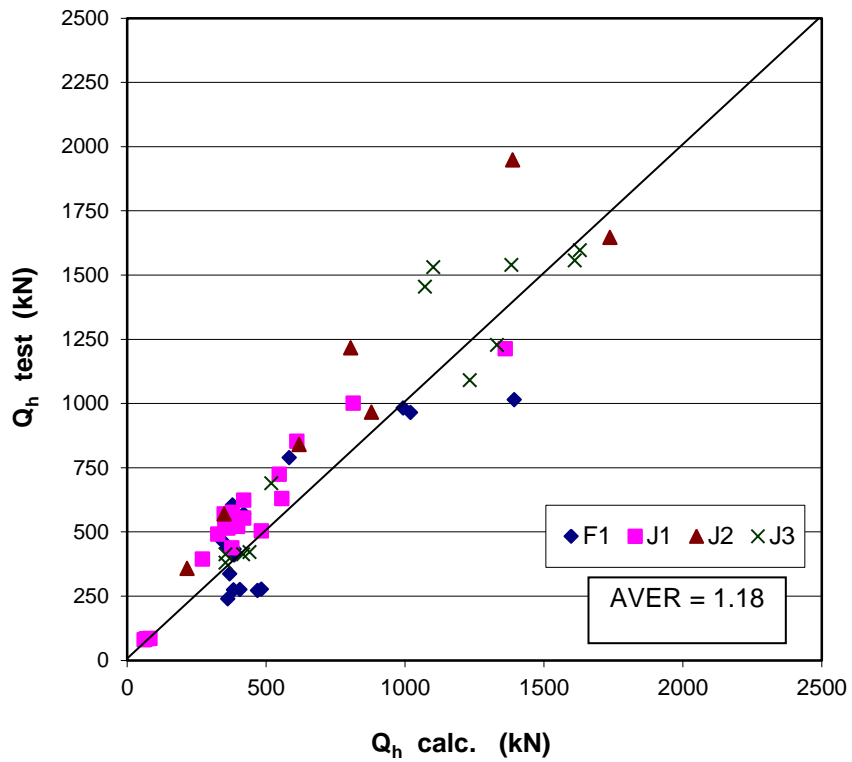
Fig.(11)- Correlation of experimental and predicted joint shear strengths for interior joints
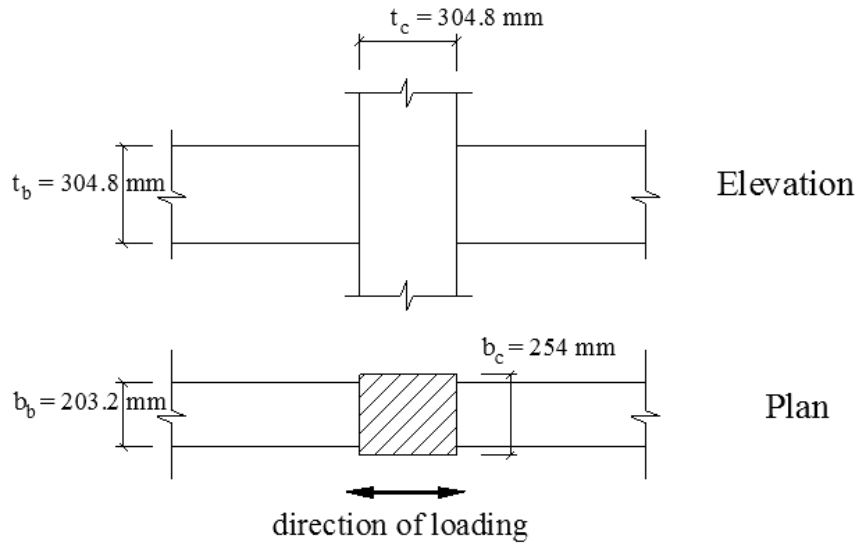
Fig.(12)- The standard specimen
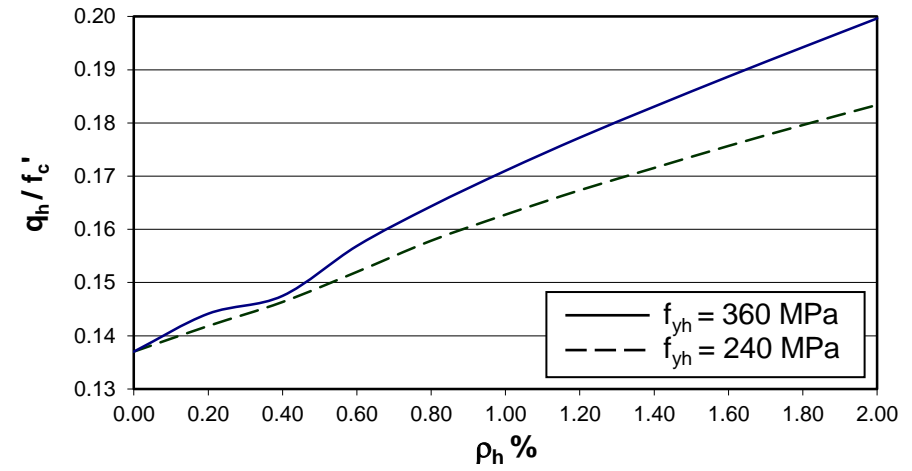
Fig.(13)- Effect of horizontal steel type and ratio
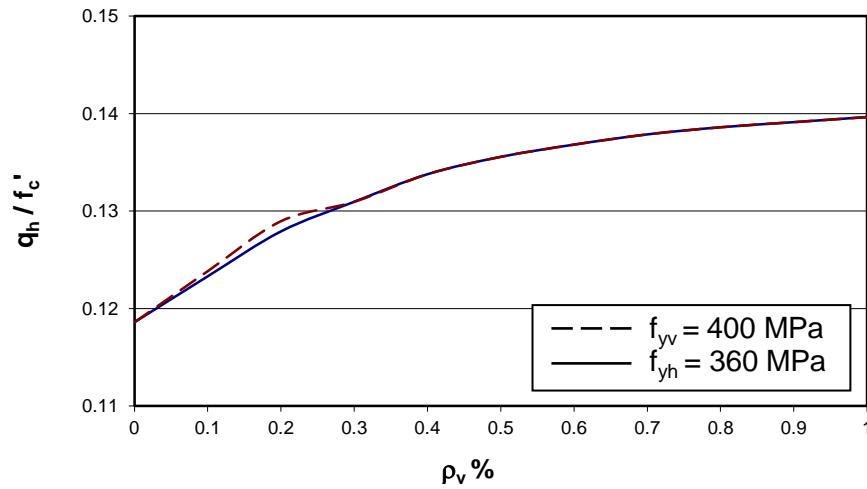
Fig.(14)- Effect of vertical steel type and ratio
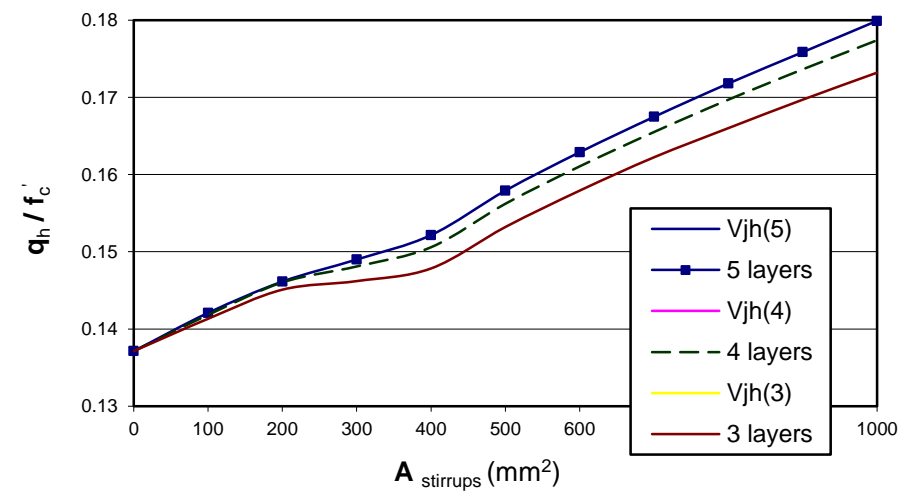
Fig.(15)- Effect of distribution pattern of joint stirrups
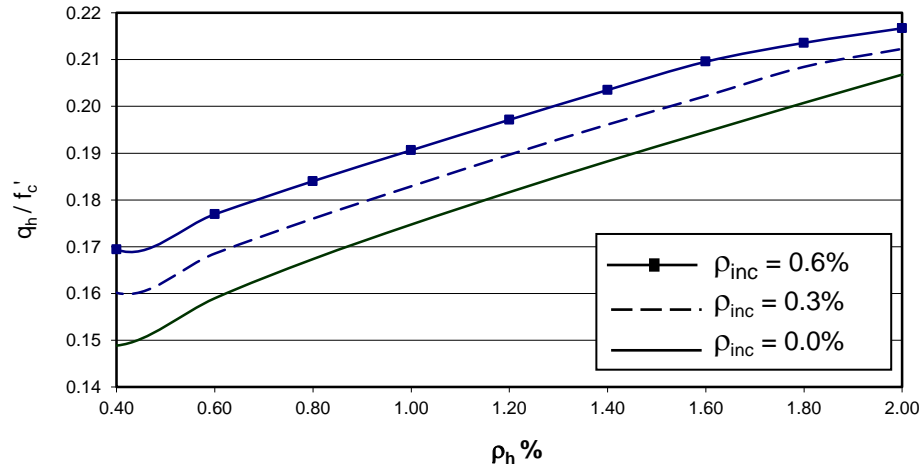
Fig.(16)- Effect of cross inclined bars
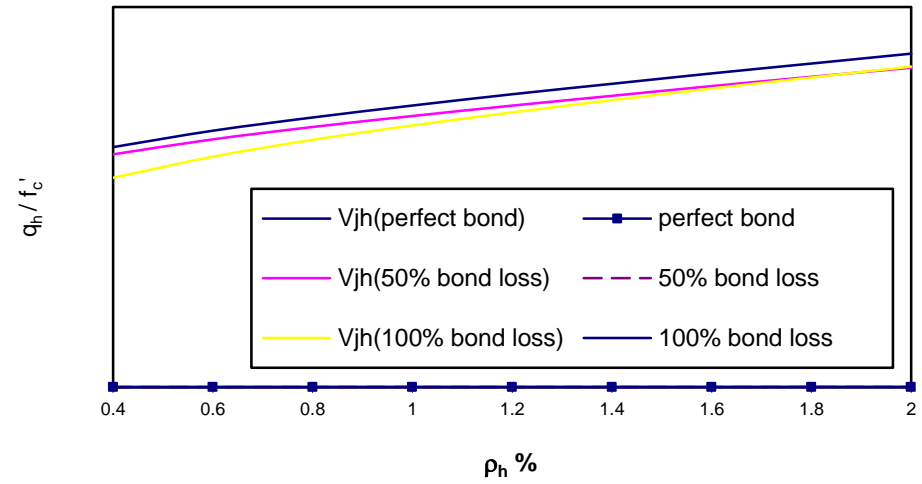
Fig.(17)- Effect of bond slip of interior joint reinforcement
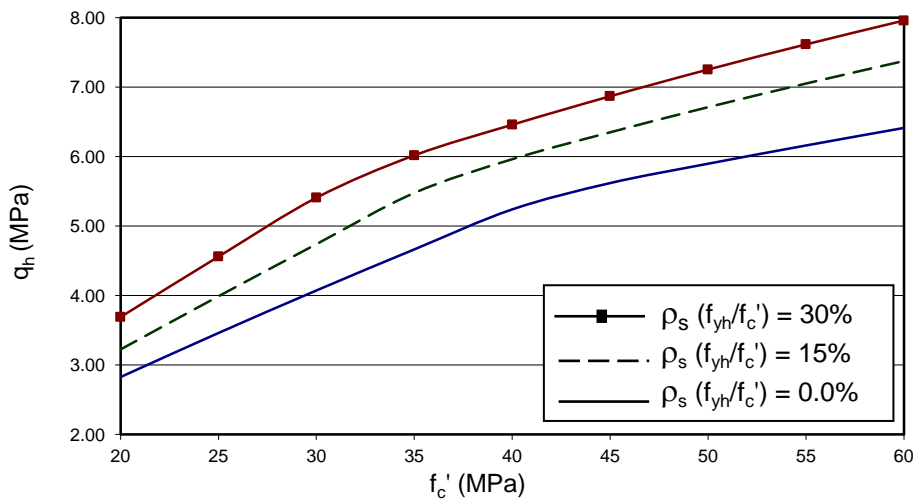
Fig.(18)- Effect of concrete strength and confinement
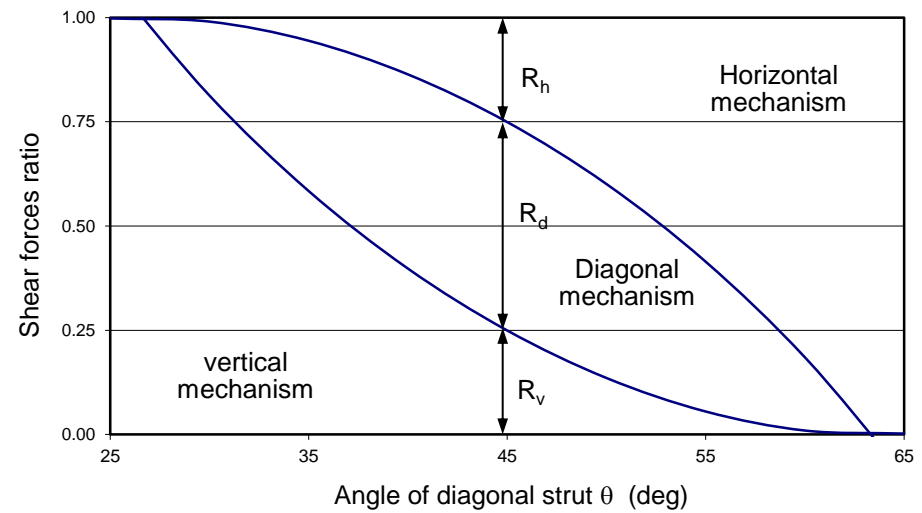
Fig.(19)- Distribution ratios of shear forces among resisting mechanisms
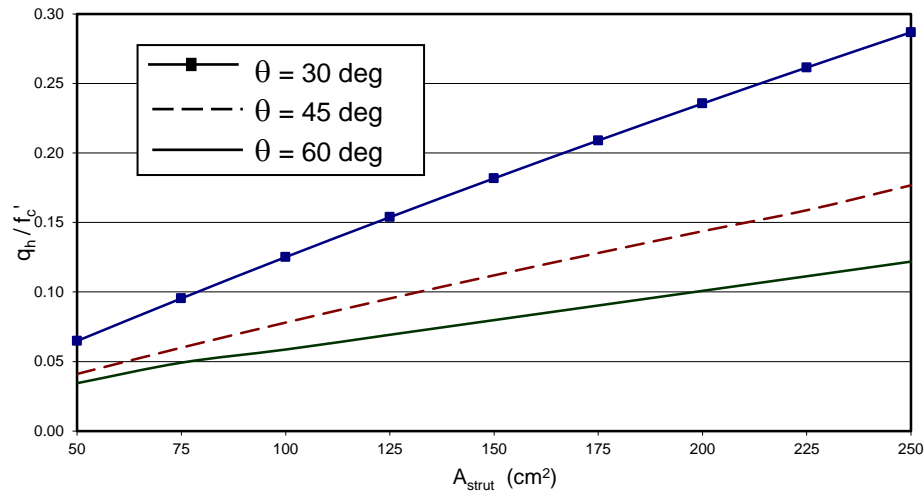
Fig.(20)- Effect of area and inclination of diagonal strut
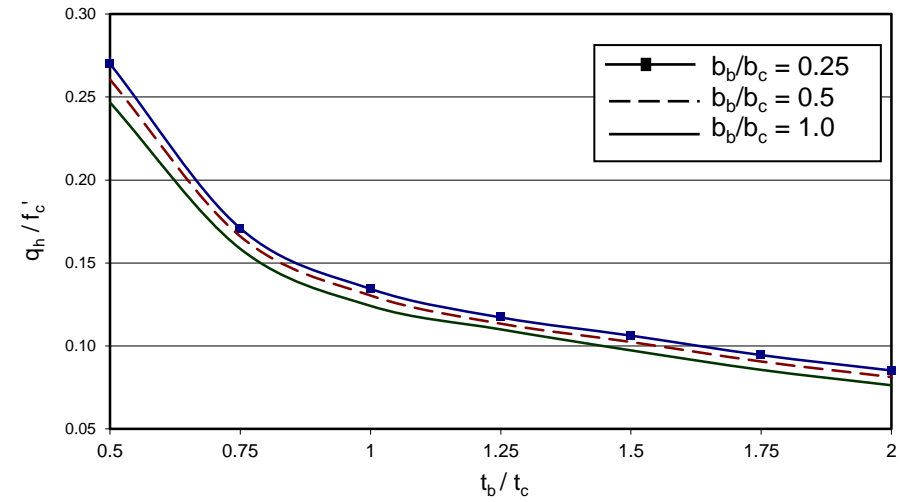
Fig.(21)- Effect of joint geometry aspect ratio
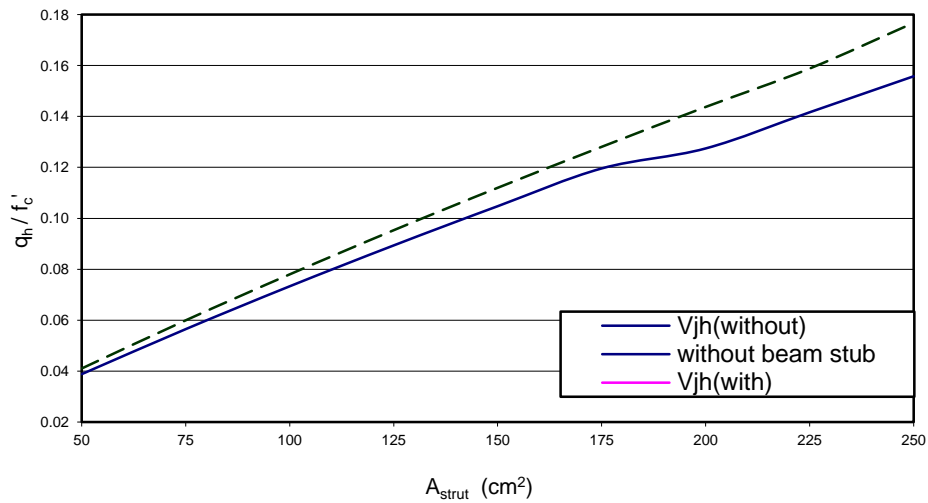
Fig.(22)- Effect of beam stub at exterior joint

Fig.(23)- Effect of column load level and type